Characterization of Vis Toxin, a Novel ADP-Ribosyltransferase from Vibrio splendidus

ARTICLE *in* BIOCHEMISTRY · SEPTEMBER 2015

Impact Factor: 3.02 · DOI: 10.1021/acs.biochem.5b00921

8 AUTHORS, INCLUDING:

Miguel R. Lugo

University of Guelph

21 PUBLICATIONS **233** CITATIONS

SEE PROFILE

Emil F Pai

University of Toronto

201 PUBLICATIONS **10,704** CITATIONS

SEE PROFILE

BIOCHEMISTRY
including biophysical chemistry & molecular biology

Article

pubs.acs.org/biochemistry

Characterization of Vis Toxin, a Novel ADP-Ribosyltransferase from *Vibrio splendidus*

Ravikiran Ravulapalli,[†] Miguel R. Lugo,[†] Roland Pfoh,[∥,⊥,@] Danielle Visschedyk,[†] Amanda Poole,[†] Robert J. Fieldhouse,[‡,§] Emil F. Pai,[⊥,@,#] and A. Rod Merrill*[,†]

[†]Department of Molecular and Cellular Biology, University of Guelph, Guelph, Ontario, Canada N1G 2W1
[‡]Computational Biology Center, Memorial Sloan-Kettering Cancer Center, New York, New York 10065, United States
[§]Department of Systems Biology, Harvard Medical School, Boston, Massachusetts 02115, United States
[∥]Department of Biology, York University, Toronto, ON, Canada M3J 1P3
[⊥]Department of Biochemistry, University of Toronto, Toronto, ON, Canada M5S 1A8
[@]Campbell Family Institute for Cancer Research, Princess Margaret Hospital, Toronto, ON, Canada M5G 1L7
[#]Departments of Medical Biophysics and Molecular Genetics, University of Toronto, Toronto, ON, Canada M5S 1A8

ABSTRACT: Vis toxin was identified by a bioinformatics strategy as a putative virulence factor produced by *Vibrio splendidus* with mono-ADP-ribosyltransferase activity. Vis was purified to homogeneity as a 28 kDa single-domain enzyme and was shown to possess NAD^+-glycohydrolase [$K_{M(NAD^+)}$ = 276 ± 12 μM] activity and with an R-S-E-X-E motif; it targets arginine-related compounds [$K_{M(agmatine)}$ = 272 ± 18 mM]. Mass spectrometry analysis revealed that Vis labels L-arginine with ADP-ribose from the NAD^+ substrate at the amino nitrogen of the guanidinium side chain. Vis is toxic to yeast when expressed in the cytoplasm under control of the CUP1 promotor, and catalytic variants lost the ability to kill the yeast host, indicating that the toxin exerts its lethality through its enzyme activity. Several small molecule inhibitors were identified from a virtual screen, and the most potent compounds were found to inhibit the transferase activity of the enzyme with K_i values ranging from 25 to 134 μM. Inhibitor compound M6 bears the necessary attributes of a solid candidate as a lead compound for therapeutic development. Vis toxin was crystallized, and the structures of the apoenzyme (1.4 Å) and the enzyme bound with NAD^+ (1.8 Å) and with the M6 inhibitor (1.5 Å) were determined. The structures revealed that Vis represents a new subgroup within the mono-ADP-ribosyltransferase toxin family.

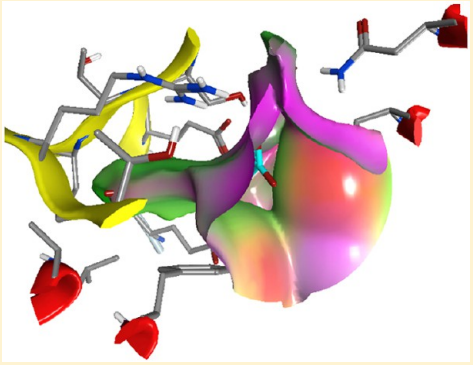

Vibrio splendidus is a curved rod-shaped, Gram-negative bacterium that possesses flagella and belongs to the Vibrionaceae family. It is known to participate in diseases involving mollusks.[1] Similar to many *Vibrio* species, *V. splendidus* is a ubiquitous marine bacterium frequently found in association with organisms ranging from plankton to fish.[2,3] Animal associations have also been observed, encompassing commensal to pathogenic interactions depending on both host and strain identities.[5,6] One particular *V. splendidus* strain, 12B01, has emerged as a problem for shellfish industries, where infection of *Crassostrea gigas* (Pacific oyster) often results in oyster mortality leading to substantial economic losses.[3] *C. gigas* fatality due to *Vibrio* infection is poorly understood and may be caused by *V. splendidus* 12B01 virulence factors, including toxin production.

The mono-ADP-ribosyltransferase enzymes (mARTs) are the principle causative agents of a number of diseases, including cholera, diphtheria, and whooping cough.[4,5] These toxic proteins bind NAD^+, cleave it into ADP-ribose and nicotinamide components, and facilitate the covalent transfer of the ADP-ribose to a host cell protein target (usually), altering or inhibiting target activity. Because of this covalent addition, mART toxins may be solely responsible for or may contribute to the disease state caused by their native pathogenic bacteria. Toxins of this family have distinct and varied substrates, and even the protein residue modified is not consistent. mART enzymes lack global primary sequence homology but share a conserved fold pattern (SCOP code d.166.1.1) in the catalytic domain, and hallmark catalytic residues in the active site.[5] Specifically, (i) a catalytic Arg preceded by an aromatic residue aids in NAD^+ binding and scaffolding of the active site, (ii) a Ser-Thr-Ser motif on a β-strand stabilizes the NAD^+-binding site, (iii) the ADP-ribosyl-turn-turn (ARTT) loop contains a catalytic Glu responsible for the mART activity and a Gln/Glu motif two residues upstream may participate in substrate recognition, and (iv) a "phosphate nicotinamide" or PN loop contributes to NAD^+ binding through hydrogen bonds with an Arg and aromatic residues. Historically, mART toxins have been divided into the

Received: June 10, 2015
Published: September 9, 2015

DOI: 10.1021/acs.biochem.5b00921
Biochemistry 2015, 54, 5920−5936

diphtheria-like (DT group) and cholera toxin-like (CT group) groups but can be further divided on the basis of their target substrate, or domain organization.[5,6] Among others, the actin-targeting toxins include C2 toxin from *Clostridium botulinum*,[7] iota toxin from *Clostridium perfringens*,[8] VahC from *Aeromonas hydrophila*,[9] and Photox from *Photorhabdus luminescens*.[10] These mART toxins share a secondary catalytic Glu residue on the ARTT loop and are usually AB binary toxins consisting of a mART domain and a cell-binding domain. By contrast, the C3-like toxins are small single-domain enzymes targeting Rho GTPases. Examples include C3bot1 and C3bot2 from *Cl. botulinum*,[11,12] C3lim from *Clostridium limosum*,[13] and C3stau1, C3stau2, and C3stau3 from *Staphylococcus aureus*.[14−16] Structures and biochemical data have allowed reaction mechanisms to be proposed for several mARTs.[17−21] Further identification and characterization of new mART toxins are improving our collective understanding of how these enzymes work and, as a result, how to inhibit them and treat infections caused by the offending pathogens.

In silico analysis has revealed a putative novel mART toxin, herein named Vis (UniProt entry A3UNN4), in vibriosis-causing *V. splendidus* strain 12B01.[22] Similar proteins exist in *Vibrio harveyi* strains HY01 and BB120, *Photobacterium* sp. SKA34, and *Photobacterium angustrum* S14. Vis is a single-domain toxin with 249 residues and is a 28 kDa protein harboring a secretion signal peptide. We have cloned, purified, and characterized this enzyme to show that it is a mART enzyme with both glycohydrolase (GH) and transferase (mART) activities. Vis toxin expression in yeast, driven by the CupI promoter, shows cell death in the presence of the wild-type (WT) toxin, and the catalytic signature variants are not toxic in yeast. We have characterized the NAD^+ binding properties of Vis toxin and tested an in-house library of compounds (the M-series) that allowed us to identify several inhibitors against Vis enzyme activity. We present the first crystal structures of Vis in apo form (Vis-apo) and in complex with substrate (Vis-NAD^+), along with the structure of small molecule, active-site inhibitor M6 (Vis-M6). Although Vis shows a fold recognition matching that of iota I_a toxin [Protein Data Bank (PDB) entry 1GIQ], it is clear that Vis represents a new subgroup in the mART toxin family.[6,22] However, its endogenous target protein remains elusive.

EXPERIMENTAL PROCEDURES

Unless otherwise noted, chemicals were purchased from Sigma-Aldrich (St. Louis, MO).

Cloning, Expression, and Purification of Vis. Multiple constructs were designed for expression of the recombinant Vis protein. The gene encoding Vis was amplified by polymerase chain reaction and subcloned into expression vector pET28-MHL, which encodes an N-terminal 20-residue sequence that contains a hexahistidine tag (His_6 tag) and a thrombin cleavage site (MGSSHHHHHHSSGLVPRLGS). All recombinant constructs were tested for expression in *Escherichia coli* strain BL21(DE3) (Stratagene) grown at 37 °C and induced overnight with 1.0 mM isopropyl 1-thio-β-D-galactoside (IPTG) at 16 °C. The truncated version of the 249-residue Vis protein (V12B01_18061), Pro^{20}−Ala^{240}, which lacked the secretion signal peptide (residues 1−19) and had nine disordered residues removed from the C-terminus, was produced in *Escherichia coli*. This recombinant construct was further used for large-scale expression in 4 L cultures of 2×YT containing kanamycin (30 μg/mL). Harvested cells were resuspended in 50 mM Tris (pH 7.5), 500 mM NaCl, and 10% glycerol (lysis buffer) and lysed by sonication. Following centrifugation at 14000*g* for 50 min, the supernatant was loaded to a Zn^{2+}-charged HiTrap Chelating HP column (GE Healthcare, Mississauga, ON) equilibrated with 50 mM TAPS (pH 8.5), 500 mM NaCl, 2% glycerol, and 10 mM imidazole, and the proteins were eluted with a 0 to 250 mM imidazole gradient. Samples were assessed for purity via Coomassie staining by sodium dodecyl sulfate−polyacrylamide gel electrophoresis (SDS−PAGE). Size-exclusion chromatography on Superdex 200 (GE Healthcare) was conducted to improve the purity of the Vis protein. The gel filtration column was equilibrated with 25 mM TAPS (pH 8.5), 500 mM NaCl, 50 mM histidine, and 5% glycerol. The eluted pure protein was concentrated by using an Amicon Ultra-15 10 kDa filter (Millipore, Billerica, MA) to ∼3 mg/mL. The FLAG tag version of recombinant Vis was generated by transferring the truncated Vis construct into the pT7-FLAG plasmid (Sigma-Aldrich). The FLAG-tagged Vis protein was expressed and purified as described above for the wild-type (WT) native Vis toxin.

Immunoblotting. The Vis sample was separated by electrophoresis on 8 to 12% SDS−polyacrylamide gels and transferred to polyvinylidene fluoride membranes (Millipore) using a semidry transfer unit (Bio-Rad). Membranes were blocked in 5% BSA in phosphate-buffered saline (PBS) for at least 1 h before antibody incubation. Blots were washed three times for 5 min each in PBS after treatment with the horseradish peroxidase-conjugated primary antibody (24 h, 4 °C with nutation) and visualized with ECL chemiluminescence detection reagent (Thermo Scientific) and film.

Liquid Chromatography−Mass Spectrometry of L-Arginine. Liquid chromatography and mass spectrometry analyses were performed in the Mass Spectrometry Facility within the Advanced Analysis Centre at the University of Guelph. Samples were injected into a Dionex UHPLC UltiMate 3000 liquid chromatograph interfaced with an amaZon SL ion trap mass spectrometer (Bruker Daltonics, Billerica, MA). A Luna C18 column (5 μm particle size, 150 mm × 2 mm; Phenomenex, Torrance, CA) was used for chromatographic separation. The initial mobile phase conditions were 100% water (0.1% formic acid) isocratic for 5 min followed by a gradient to 60% acetonitrile (0.1% formic acid) in 20 min then a single-step gradient to 100% acetonitrile over 10 min. The flow rate was maintained at 0.4 mL/min. The mass spectrometer electrospray capillary voltage was maintained at 4.5 kV and the drying gas temperature at 280 °C with a flow rate of 10 L/min. The nebulizer pressure was 40 psi. Nitrogen was used as both the nebulizing gas and the drying gas, and helium was used as the collision gas at 60 psi. The mass spectrometer was set on enhanced resolution positive-ion auto MS/MS mode and scanned from m/z 50 to 1500. The Smart Parameter Setting (SPS) was used to automatically optimize the trap drive level for selected precursor ions. The instrument was externally calibrated with the ESI TuneMix (Agilent Technologies, Santa Clara, CA). The reaction product ADP-ribose-Arg was observed as both a singly and doubly charged ion at m/z 716 and 358.5, respectively.

Crystallization, Data Collection, and Refinement of Vis and Vis-Inhibitor/Substrate Complexes. Purified Vis protein (1.4 mg/mL) was crystallized using the hanging-drop vapor-diffusion method. The reservoir solution contained 30% Jeffamine ED-2001 (0.1 M, pH 7.0). Equal volumes (4 μL) of a

DOI: 10.1021/acs.biochem.5b00921
Biochemistry 2015, 54, 5920−5936

Table 1. Crystallographic Data and Refinement Statistics for *V. splendidus* Vis Structures

	Vis-apo	Vis-NAD$^+$	Vis-M6
	Diffraction		
PDB entry	4Y1W	4XZJ	4YC0
X-ray source	CLS beamline 08ID	Rigaku Micromax-007 HF	CLS beamline 08ID
wavelength (Å)	0.9762	1.54178	0.9762
unit cell parameters (Å)	a = 48.50	a = 49.70	a = 48.23
	b = 51.80	b = 52.00	b = 52.16
	c = 102.80	c = 100.40	c = 101.60
space group	$P2_12_12_1$	$P2_12_12_1$	$P2_12_12_1$
resolution range (Å)[a]	35.40−1.40 (1.45−1.40)	18.63−1.80 (1.90−1.80)	46.4−1.5 (1.55−1.50)
data completeness (%)	97.7 (83.5)	94.8 (91.9)	99.98 (100)
R_{merge} (%)	6.3 (10.6)	4.45 (18.0)	9.3 (50.3)
redundancy	6.5 (3.4)	6.3 (5.2)	7.2 (7.2)
average $I/\sigma(I)$	14.7 (1.2)	25.8 (8.7)	13.0 (4.0)
	Refinement		
molecular replacement model	Vis-apo with iodide soaks	Vis-apo	Vis-apo
R_{work} (%),[b] R_{free} (%)[c]	15.6, 18.5 (26.7, 29.2)	17.5, 20.5 (21.2, 24.1)	16.3, 18.5 (21.3, 22.8)
no. of atoms			
protein	1734	1755	3451
ligand	−	44	22
water	273	145	315
rmsd from ideal			
bond lengths (Å)	0.010	0.011	0.009
bond angles (deg)	1.23	1.42	1.18
B factor (Å^2)			
protein	24.6	23.5	21.1
ligand	−	18.4	14.7
Wilson	16.7	23.0	15.2
Ramachandran plot (%)			
favored	99	100	99
outliers	0	0	0

[a]Values in parentheses are for the highest-resolution shell. [b]$\sum||F_{obs}| - |F_{calc}||\sum|F_{obs}|$, where $|F_{obs}|$ and $|F_{calc}|$ are the observed and calculated structure factor amplitudes, respectively. [c]The R_{free} value was calculated with a random 5% subset of all reflections excluded from refinement.

protein solution and a reservoir solution were mixed for crystallization. All crystals grew to a mountable size in 4−5 days. Crystals were soaked in the corresponding mother liquor supplemented with 15% glycerol as a cryoprotectant before being frozen in liquid nitrogen. The crystals used for solving phase information were soaked for a few seconds in mother liquor (2 mL) supplemented with 0.15 g of potassium iodide. Diffraction data for potassium iodide-soaked crystals were originally collected at the Structural Genomics Consortium (Toronto, ON). They were reduced in XDS/XScale and merged in Xprep, and the structure was determined with Shelx-SAD. This structure was then refined against 1.40 Å resolution data collected later at the Canadian Light Source with Phenix[23] applying TLS and 2-fold NCS restraints.

Vis-NAD$^+$ Structure. Crystals of Vis-apo were soaked in their mother liquor containing 1.3 mM NAD$^+$ and 15% glycerol for 60 s and then flash-cooled in liquid nitrogen. Data were collected on a Rigaku diffractometer (rotating Cu anode) using multilayer optics and a Mar-345 image plate detector at a temperature of 100 K. Data processing was conducted with XDS.[24] It was possible to determine the structure with PHASER using the structure of Vis-apo as the search model. The structure was refined with Refmac[25] against 1.8 Å resolution data, and model adjustment was performed in Coot.[26]

Vis-M6 Structure. For the Vis complex with M6, the inhibitor was soaked into crystals by first transferring the crystal to a 4 μL drop of a reservoir solution for 5 min. Then inhibitor M6 was added to a final concentration of 1 mM and the mixture incubated for 3 h. The diffraction data were collected at the Canadian Macromolecular Crystallography Facility (CLS, 08ID-1) and are listed in Table 1. The data were processed in XDS.[24] Table 1 lists data collection and final model refinement statistics for all data sets and models. All manual model building was performed with COOT.[26] Structure figures were prepared using PyMOL (The PyMOL Molecular Graphics System, version 1.5.0.4, Schrödinger, LLC) and Molecular Operative Environment (MOE) release 2014.08 (Computational Chemistry Group, 2014). Structure factors and coordinate sets for Vis-apo, Vis-NAD$^+$, and Vis-M6 have been deposited in the Protein Data Bank as entries 4Y1W, 4XZJ, and 4YC0, respectively.

Vis GH and mART Activity. Vis GH measurements were performed using a FLUOstar Omega plate reader (BMG, Ortenberg, Germany) with the fluorescent NAD$^+$ analogue, etheno-NAD$^+$ (εNAD$^+$). Cleavage of the bond between nicotinamide and etheno-ADP-ribose (εADP-ribose) causes a 10-fold increase in the fluorescence quantum yield of the etheno group by reducing the level of intramolecular quenching.[27] For GH activity, 10 μM Vis was combined with various concentrations (0−600 μM) of εNAD$^+$ in reaction buffer [25 mM Tris-HCl and 500 mM NaCl (pH 7.9)] and the reactions were monitored for 4 h at 25 °C with excitation and emission filters of 300 and 405 nm, respectively. The samples

DOI: 10.1021/acs.biochem.5b00921
Biochemistry 2015, 54, 5920−5936

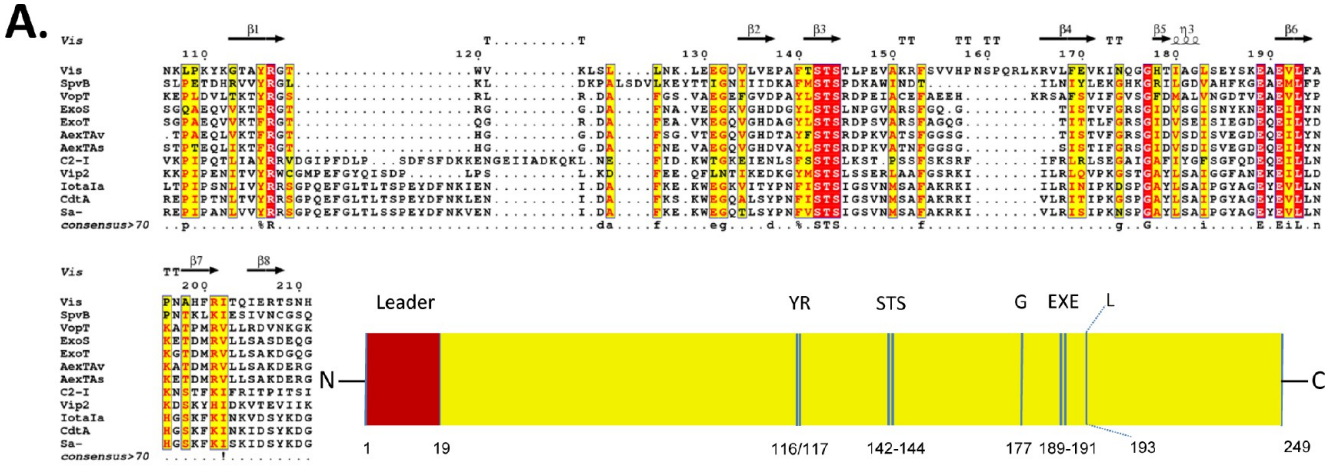

B.

	Vis	VopT	ExoS	ExoT	AexTAv	AexTAs	SpvB	C2-I	Vip2	Iota Ia	CdtA	Sa
Vis	100	28	25	21	21	22	23	22	14	19	20	21
VopT	28	100	40	43	45	46	23	16	21	23	27	26
ExoS	25	40	100	76	73	71	18	24	23	24	23	23
ExoT	21	43	76	100	77	74	20	22	22	23	25	23
AexTAv	21	45	73	77	100	88	21	25	20	23	23	23
AexTAs	22	46	71	74	88	100	21	23	22	24	23	24
SpvB	23	23	18	20	21	21	100	24	26	24	24	24
C2-I	22	16	24	22	25	23	24	100	30	33	31	30
Vip2	14	21	23	22	20	22	26	30	100	42	41	41
Iotala	19	23	24	23	23	24	24	33	42	100	88	86
CdtA	20	27	23	25	23	23	24	31	41	88	100	91
Sa	21	26	23	23	23	24	24	30	41	86	91	100

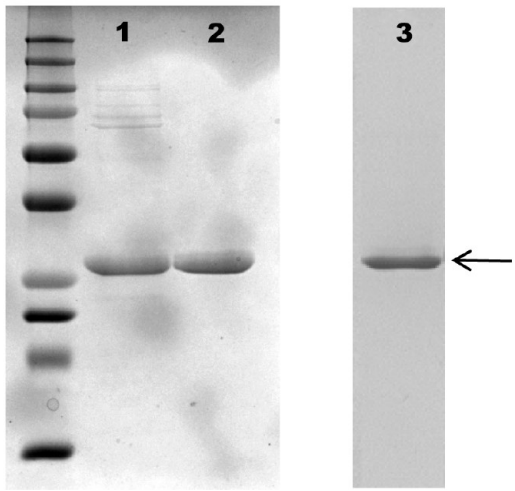

Figure 1. Multiple-sequence alignment of Vis with various ExoS-like and C2-like mART toxins. (A) Sequence alignment of Vis with some ExoS-like and C2-like toxins produced using the T-Coffee web server to align the sequences and ESPript to generate the alignment figure.[57] Key catalytic regions are highlighted, and the numbering is for the catalytic core only. Identical residues are highlighted in red, and similar residues are shown with red text. A cartoon sequence of full length Vis is colored yellow (1−249) with the N-terminal leader sequence colored red (1−19). Other sequence elements are Y-R (116 and 117), S-T-S (142−144), conserved Gly (177), essential E-X-E (189−191), and conserved Leu (193). (B) Identity matrix showing the amino acid identity among the 100 core catalytic residues of the known ExoS-like, C2-like toxins and Vis. Salmon indicates highly diverse sequences; light green indicates a large amount of conservation, and yellow indicates an intermediate level of conservation among sequences. The identity matrix was generated using ClustalX2[58] and colored using Microsoft Excel. (C) Purification and identification of Vis toxin from *E. coli* lysate. SDS−PAGE gel and anti-His tag Western blot showing the purification and identification of Vis: molecular mass standards at 10, 15, 20, 25, 37, 50, 75, 100, 150, and 250 kDa; lane 1, Vis protein after IMAC purification; lane 2, purified Vis protein after gel filtration chromatography; lane 3, Western blot, purified Vis. The arrow indicates the position of Vis toxin.

DOI: 10.1021/acs.biochem.5b00921
Biochemistry 2015, 54, 5920−5936

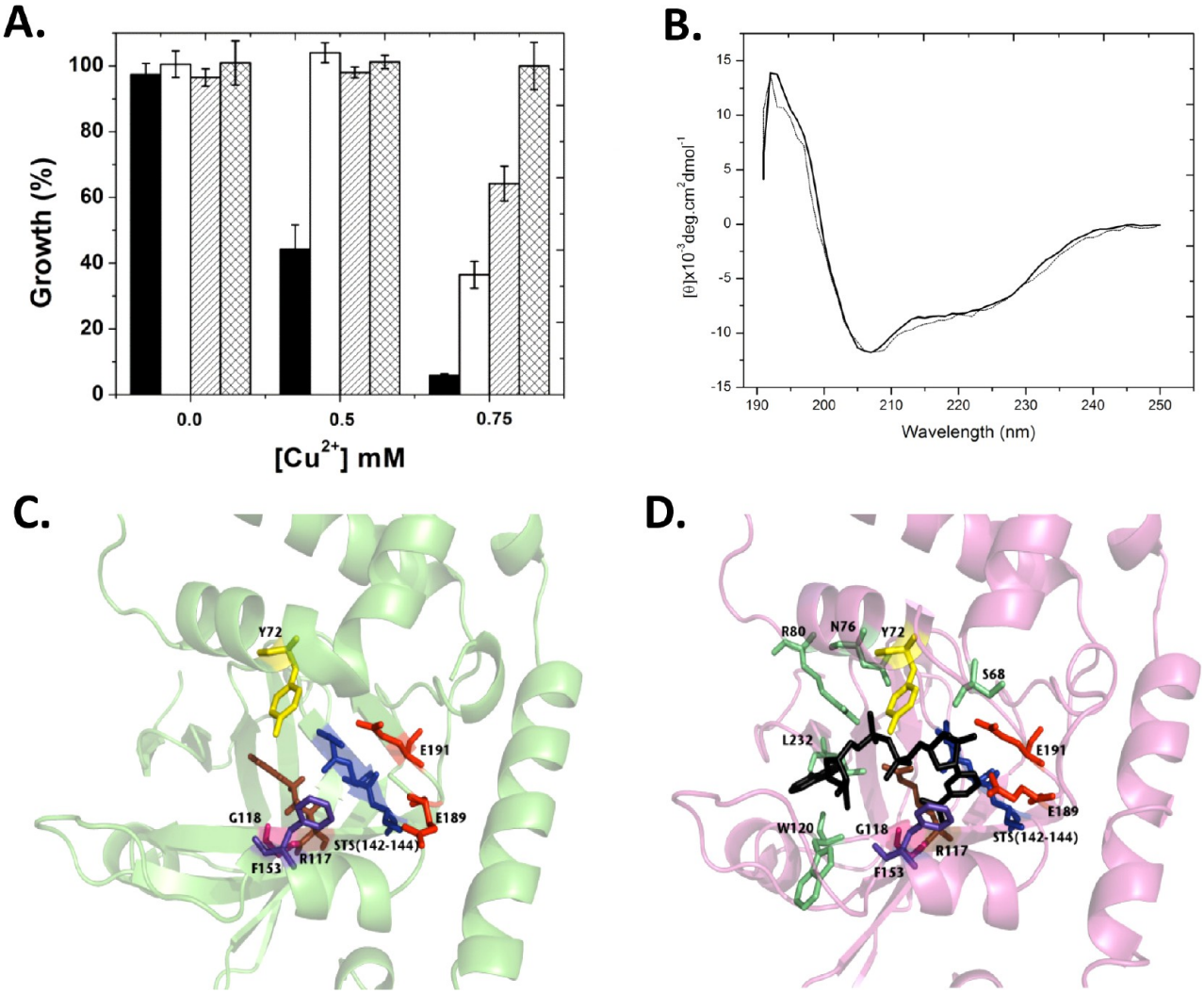

Figure 2. Vis inhibition of yeast growth, substrate binding, and Vis-apo and Vis-NAD$^+$ structures. (A) Inhibition of yeast growth by Vis and selected catalytic variants. All growth is compared to that of yeast expressing a nontoxic protein as control (*St. aureus* aminotransferase). Growth is shown at three different concentrations of Cu^{2+} induction, indicated on the abscissa: black bar, Vis WT; white bar, Vis Q189A variant; fine stripes, Vis E191A variant; grid pattern, Vis Q189A/E191A. (B) CD spectra of Vis wild-type (thick line) and E189A/E191A (thin dotted line) in 25 mM Tris, 500 mM NaF buffer (pH 7.5). The concentrations of the proteins were both at 0.13 mg/mL, and each spectrum is the average of six independent spectra. (C) Close-up of the Vis-apo crystal structure shown as a ribbon diagram. Catalytic residues Arg^{117}, Ser^{142}, and Glu^{191} are colored brown, blue, and red, respectively. Other important residues in the reaction mechanism, Tyr^{72} (yellow), Glu^{189} (red), STS motif (blue), Gly^{118} (pink), and Phe^{153} (purple), are also highlighted. (D) Vis-NAD$^+$ complex structure shown as a ribbon diagram. NAD$^+$ is colored black and represented in stick format. Important residues that coordinate with NAD$^+$ through hydrogen bonds are highlighted. Arg^{80}, Asn^{76}, Trp^{120}, and Leu^{132} are colored green.

were loaded into a 96-well Grenier half-area clear plate (Corning, Corning, NY), with a final reaction volume of 50 μL, and sealed with clear tape. Initial sample slopes were measured and converted from the fluorescence rate of change (arbitrary units per minute) to the concentration rate of change (micromolar per minute) using a known standard solution of εAMP in a calibration curve.

For mART activity, Vis (9.5 μM) was combined with εNAD$^+$ (0−600 μM) (at 640 mM agmatine) or with agmatine (0−800 mM) (at 400 μM εNAD$^+$), accordingly, in reaction buffer [25 mM Tris-HCl (pH 7.5), 500 mM NaCl, 5% glycerol, and 2 mM DTT] at 25 °C. The reaction was monitored for 1 h with excitation and emission filters of 300 and 405 nm, respectively. All the kinetic data were fit using nonlinear regression to the Michaelis−Menten equation [$v_o = V_{max}[S]/(K_M + [S])$], using GraphPad Prism version 5 (GraphPad, La Jolla, CA).

Yeast Growth-Defect Phenotypic Screen. *Saccharomyces cerevisiae* W303 (*MATa, his3, ade2, leu2, trp1, ura3, can1*) was grown on yeast-peptone-dextrose or synthetic dextrose (SD) medium. The gene encoding Vis toxin was cloned in *S. cerevisiae* under the transcriptional control of the CUP1 promoter on a low-copy number plasmid by homologous recombination. Transformants harboring the plasmid with the toxin gene were cultured overnight. The yeast culture was diluted into fresh medium (~5000 cells/mL), and 100 μL aliquots of the cells were used to seed a 96-well plate. $CuSO_4$ was added at different concentrations (0−0.75 mM). The plates were incubated at 30 °C for 48 h, and the growth densities were measured as previously described.[28]

Determination of Inhibition Constant K_i. The concentration of inhibitor that reduced enzymatic activity by 50% (IC_{50}) was measured using a fluorescence-based assay. The substrates, εNAD$^+$ and agmatine, were held at fixed

DOI: 10.1021/acs.biochem.5b00921
Biochemistry 2015, 54, 5920−5936

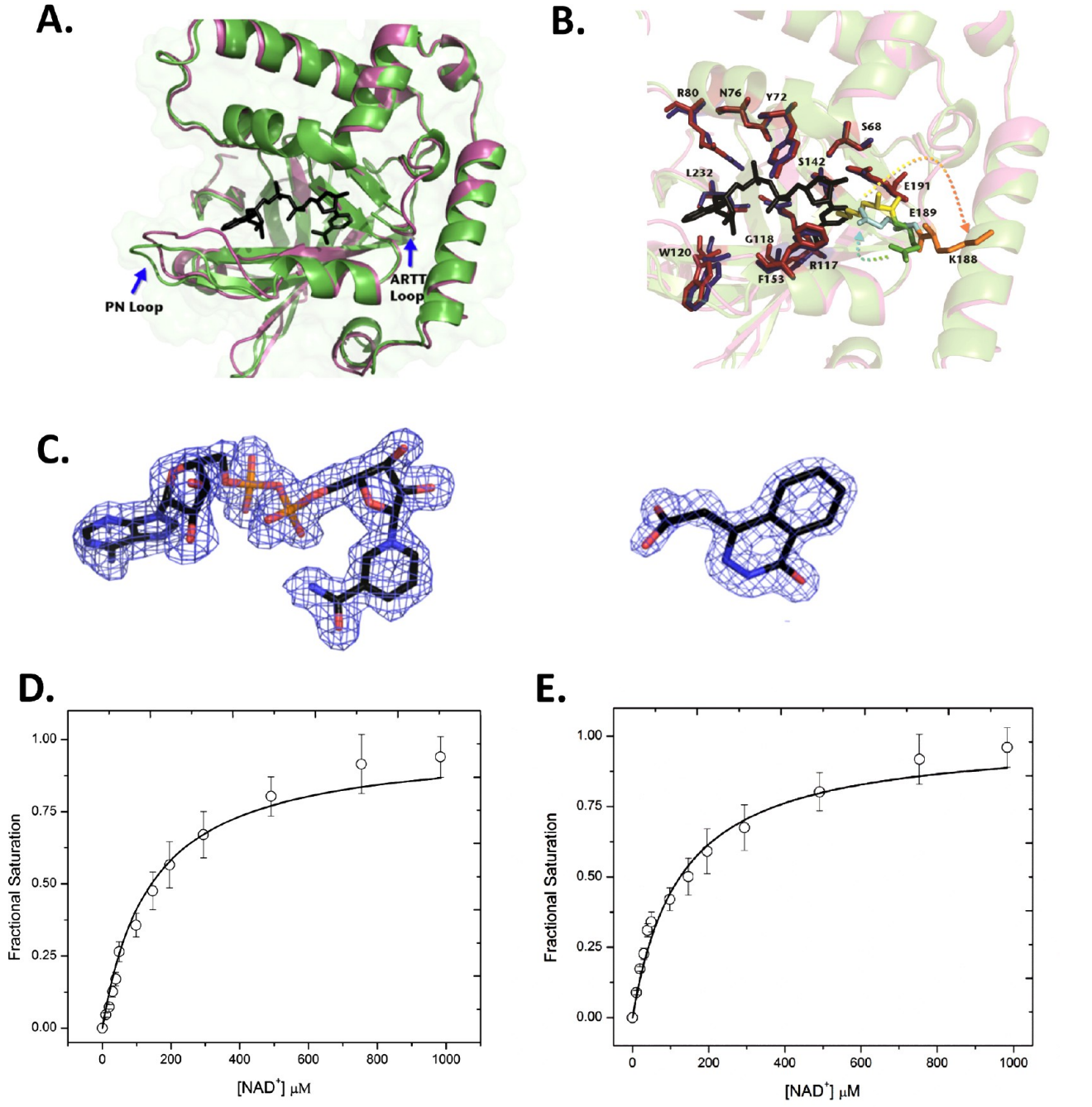

Figure 3. Comparison of Vis-apo and Vis-NAD$^+$ structures and NAD$^+$ substrate binding activity. (A) Structural comparison of Vis-apo (green) and Vis-NAD$^+$ complex structure (magenta) based on an iterative, three-dimensional alignment of protein backbone C-α atoms using PyMOL. NAD$^+$ is shown as black sticks. The PN loop and ARTT loop are highlighted by text. (B) Close-up of the active site of Vis-apo superimposed with the Vis-NAD$^+$ complex structure. Residues involved in NAD$^+$ binding are highlighted by sticks (red for Vis-apo and blue for Vis-NAD$^+$). Lys^{188} is colored yellow in the Vis-apo structure and orange in the Vis-NAD$^+$ complex structure. Glu^{189} is colored green in the Vis-apo structure and cyan in the Vis-NAD$^+$ complex structure. (C) Electron density maps of NAD$^+$ (left) and inhibitor M6 (right) bound to Vis. A simulated omit map of each of the ligands is colored blue ($2F_o - F_c$ contoured at 1δ). (D and E) NAD$^+$ binding by Vis. The excitation was at 295 nm and the emission at 340 nm, with excitation and emission band-passes at 5 nm in 5 mM Tris-HCl, 50 mM NaCl buffer (pH 7.9) at 25 °C: (D) WT Vis and (E) Q189A/E191A variant. Error bars show the SD.

concentrations of 400 μM and 640 mM, respectively, and combined with 9.5 μM Vis and increasing concentrations of inhibitor ranging from 0 to 1 mM in assay buffer [25 mM Tris-HCl (pH 7.5), 50 mM NaCl, 5% glycerol, and 2 mM DTT] to a total volume of 35 μL in a 384-well plate. The reaction was monitored using a BMG FLUOstar Omega instrument for 1 h with excitation and emission filters of 300 and 405 nm, respectively. IC_{50} values were determined by nonlinear regression curve fitting using Origin 8.0 (OriginLab, Northampton, MA). Because the IC_{50} is not a direct measure of affinity, these values were used to calculate K_i values assuming a competition model according to the Cheng−Prusoff equation:[29] $K_i = IC_{50}/(1 + [S]/K_M)$, where [S] is 400 μM εNAD$^+$ and K_M is $K_{M(\varepsilon NAD)}$ = 276 μM.

DOI: 10.1021/acs.biochem.5b00921
Biochemistry 2015, 54, 5920−5936

Measurement of Dissociation Constant K_d for NAD$^+$ and Agmatine Substrates and Competitive Inhibitors against Vis. Quenching of the intrinsic tryptophan fluorescence was used to determine the binding/dissociation constant, K_d, for both NAD$^+$ and agmatine substrates as well as for Vis inhibitors as previously described[30,31] with slight modifications. Vis toxin (1 μM) was titrated with inhibitor (0−150 μM) in 50 mM NaCl and 20 mM Tris-HCl (pH 7.9). Fluorescence was monitored using excitation and emission wavelengths of 295 and 340 nm, respectively, and bandwidths of 5 nm on a Cary Eclipse fluorescence spectrophotometer. Data were analyzed by nonlinear regression to a single-site binding equation using GraphPad Prism version 5.

Circular Dichroism of Vis. Circular dichroism (CD) spectra were acquired for Vis WT and the E189A/E191A variant in a JASCO J-815 CD spectropolarimeter (250−190 nm scan, average of six spectra). The proteins were at a concentration of 0.13 mg/mL in 25 mM Tris-HCl, 500 mM NaF buffer (pH 7.5) in a 1 mm path length UV CD cuvette at 25 °C.

RESULTS

***V. splendidus* Encodes a mART Toxin.** The 249-residue Vis protein has a molecular mass of 28 kDa and contains a 19-residue leader sequence that was removed in the protein produced in *E. coli*. Optimal expression was obtained from a construct that produced Vis with a nine-residue C-terminal truncation. Vis is a single-domain mART toxin that has the catalytic E^{189}-X-E^{191} signature characteristic of the Arg-specific mART toxins and shows the catalytic Arg^{117} residue and S^{142}-T-S^{144}- motif characteristic of the CT group (Figure 1A). Briefly, the conserved Arg^{117} binds A- or N-phosphate on NAD$^+$ and the target substrate; the conserved S-T-[SQT] motif binds the nicotinamide ring, and the conserved [QE]-X-E binds N-ribose to create a strained NAD$^+$ conformation.[22] Vis is nearly 30% identical to VopT from *Vibrio parahemolyticus* and also shows sequence similarity in the mART catalytic core with *Pseudomonas aeruginosa* ExoS and ExoT,[32] *Cl. botulinum* C2-I,[33] *Bacillus thuringiensis* Vip2,[34] and *Cl. perfringens* iota I$_a$[20] (Figure 1B). Entry of Vis into target cells is also unclear because the Vis gene encodes only a single catalytic domain. It may travel through a transporter, be aided by other pore-forming toxins, or be directly released into the cytoplasm after *V. splendidus* invasion of the host. A search of the genomic context for the Vis gene did not find an accompanying B-domain (receptor-binding) protein within the *V. splendidus* genome.

Table 2. Kinetics and Substrate Binding Affinity Parameters of Vis Toxin

parameter[a]	mean ± standard error
binding	
$K_{d(NAD)}$ (μM)	95 ± 7
$K_{d(agmatine)}$ (mM)	3.3 ± 0.2
GH activity	
$K_{M(\varepsilon NAD)}$ (μM)	276 ± 12
$k_{cat(GH)}$ (min^{-1})	(1.20 ± 0.03) × 10^{-3}
$k_{cat(GH)}/K_{M(\varepsilon NAD)}$ (M^{-1} min^{-1})	4.3
mART activity	
$K_{M(\varepsilon NAD)}$ (μM)	276 ± 12[b]
$K_{M(agmatine)}$ (mM)	272 ± 18
$k_{cat(mART)}$ (min^{-1})	(1.10 ± 0.03) × 10^{-2}
$k_{cat(mART)}/K_{M(\varepsilon NAD)}$ (M^{-1} min^{-1})	39.8
$k_{cat(mART)}/K_{M(agmatine)}$ (M^{-1} min^{-1})	0.41

[a]Kinetics and binding affinity parameters were obtained as described in Experimental Procedures and represent triplicate measurements for at least three separate experiments. [b]Assuming the same value as for the GH activity.

Expression of Vis in *E. coli*. The Vis gene was overexpressed in Rosetta *E. coli* cells, and the protein was purified at a yield of several milligrams per liter of culture using immobilized metal affinity chromatography, followed by gel filtration chromatography. The purity level was assessed by SDS−PAGE (Figure 1C, lane 2), and the protein was positively identified by Western blot analysis using an anti-His tag antibody (Figure 1C, lane 3).

Vis Is Toxic When Expressed in Yeast. Vis toxin expression in yeast, driven by the CUP1 promoter, showed cell death in the presence of the WT toxin at doses of 0.5 and 0.75 mM Cu^{2+} (Figure 2A). Almost complete growth restoration with the E189A and E191A variants and the E189A/E191A double variants was observed at 0.5 mM Cu^{2+} induction, and growth restoration occurred to a greater extent with the E189A/E191A double variant than the single variants at the highest dose of 0.75 mM Cu^{2+} (Figure 2A). The growth-defective phenotype clearly suggests that Vis is toxic to yeast as a model eukaryote. Substitutions at Glu^{189} and Glu^{191} confirm that Vis cytotoxicity can be attributed to the mART activity of the toxin and endorse its role as a bone fide mART toxin with cytotoxicity in a eukaryotic cell system.

Vis Toxin Folded Integrity. To assess the folded integrity of the enzymes, CD spectroscopy was conducted on the Vis WT and the double variant (E189A/E191A), which showed typical spectra for an α/β-type domain, and there also were no significant differences in the folding of the two proteins based on their CD spectra (Figure 2B). This indicates that Vis was properly folded and was an active enzyme and that replacement of Glu^{189} and Glu^{191} residues did not significantly perturb the folded integrity of the enzyme (Figure 2B).

Vis-apo Crystal Structure. Vis shows a fold recognition match with iota I$_a$ toxin (PDB entry 1GIQ, J$_{3D\text{-}jury}$); however, we were unable to determine the Vis structure by molecular replacement using any mART toxin structures as search models. Phases for the Vis structure were obtained from Vis crystals soaked in potassium iodide; the partial model obtained was used as a molecular replacement template to obtain a high-resolution structure. The structure of recombinant Vis was refined to a resolution of 1.40 Å in the apo (substrate-free) form (Figure 2C). The Vis protein folds into a mixed α/β domain and displays a characteristic mART fold for the CT group toxins. However, superposition of Vis with other mART toxins shows some structural differences as seen from the root-mean-square deviation (rmsd) values in key regions of the catalytic domains of iota I$_a$ (2.80 Å, PDB entry 1GIQ), VahC (3.07 Å, PDB entry 4FML), and C3Bot1 (3.81 Å, PDB entry 2C89) toxins. The PN loop (residues 146−164) that connects β-strands β3 and β4 is longer and more extended in Vis than in other CT mART toxins (iota I$_a$, C3Bot1), suggesting that Vis may interact with a unique substrate, not previously observed in this toxin family. Like VahC but unlike iota I$_a$, Vis has a shorter loop−helix region between β1 and β2. Some of the ARTT loop residues (184−186) are missing in the electron density map of Vis-apo, likely because of the flexibility of the loop, but these residues are visualized in the Vis-NAD$^+$ structure because of

DOI: 10.1021/acs.biochem.5b00921
Biochemistry 2015, 54, 5920−5936

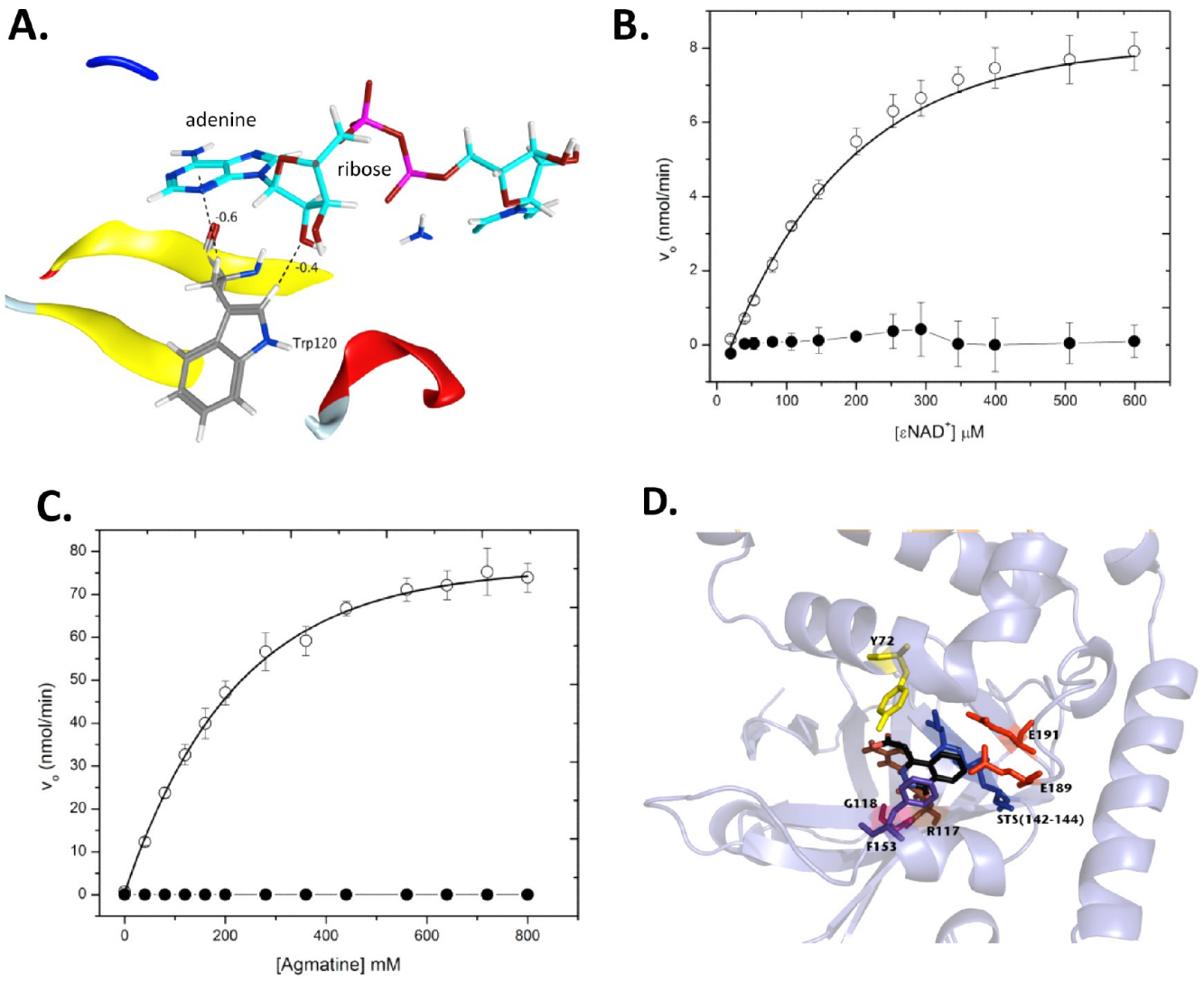

Figure 4. Vis NAD$^+$ substrate complex showing the interaction with Trp^{120}, GH, and ADP-ribosyl transferase activities and the Vis-M6 inhibitor complex. (A) Vis-NAD$^+$ substrate complex showing the interaction of Trp^{120} with the adenine and ribose rings of NAD$^+$. The calculations and visualizations were conducted with MOE2014.09 with the following settings: force field, Amber12-EHT; GB-IV solvation model (dielectric constants of 1 for protein and 80 for the aqueous solvent); cutoff switching function between 10 and 12 Å. (B) GH activity of WT and the Q189A/E191A Vis variant. Data for WT Vis are shown as empty circles and data for the Q189A/E191A Vis variant as filled circles. Error bars are the SD. (C) ADP-ribosyltransferase activity of WT and Q189A/E191A Vis variant. Vis (9.5 μM), ε-NAD$^+$ (400 μM), and agmatine (0−800 mM) were combined in reaction buffer [25 mM Tris-HCl (pH 7.5), 500 mM NaCl, 5% glycerol, and 2 mM DTT] at 25 °C as described for GH activity: WT Vis (○) and Q189A/E191A Vis variant (●). Error bars are the SD. (D) Vis-M6 complex structure. The M6 inhibitor is colored black and represented as sticks. Residues important in the reaction mechanism, Tyr^{72} (yellow), Glu^{189} (red), STS motif (blue), Gly^{118} (pink), and Phe^{153} (purple), are highlighted.

loop stabilization through ligand interactions (see the next section).

Vis-NAD$^+$ Crystal Structure. The Vis-NAD$^+$ crystal structure shows the entire NAD$^+$ molecule bound to Vis in a twisted horseshoe configuration characteristic of mART toxins (Figure 2D).[35,36] A NAD$^+$ concentration of 1.3 mM proved to be sufficient for crystal soaking, and the clearly defined electron density for NAD$^+$ supports the tight binding affinity determined by our biochemical analysis (see below). The NAD$^+$-bound structure of recombinant Vis was refined to a resolution of 1.80 Å (Figure 2D; the electron density map for NAD$^+$ is shown in Figure 3C). It shows a low rmsd from Vis-apo (0.327 Å for 152 residues). As expected, the catalytic residues within the ARTT loop orient toward the nicotinamide region of NAD$^+$ (Figure 2D). In the Vis-apo structure, the amino group of Lys^{188} occupies the N-site (Figure 2C). Upon binding NAD$^+$, Lys^{188} rotates 180°, resulting in repositioning of Glu^{189} closer to the N-ribose C1 atom of NAD$^+$ (Figure 3A,B). However, the dominant catalytic residue, Glu^{191}, and other conserved residues that interact with NAD$^+$ (Ser^{68}, Asn^{76}, Arg^{80}, Arg^{117}, and Gly^{118}) do not significantly change position upon NAD$^+$ binding (Figure 3B). Notably, the PN loop does orient more toward the NAD$^+$ molecule when this substrate binds (Figure 3A). Overall, the binding of NAD$^+$ in the Vis-NAD$^+$ structure follows a trend similar to those of previously known mART enzymes.[35,37,38] Several conserved residues bind to the A-phosphate (Asn^{76}, Arg^{80}, and Arg^{117}), N-ribose (Ser^{68} and Glu^{191}), and nicotinamide (Gly^{118}) in the NAD$^+$ substrate. In summary, there is little variation in the NAD$^+$-binding pose compared with those of other mART-NAD$^+$ complexes, except for the orientation of the adenine ring, which in Vis is stabilized

DOI: 10.1021/acs.biochem.5b00921
Biochemistry 2015, 54, 5920−5936

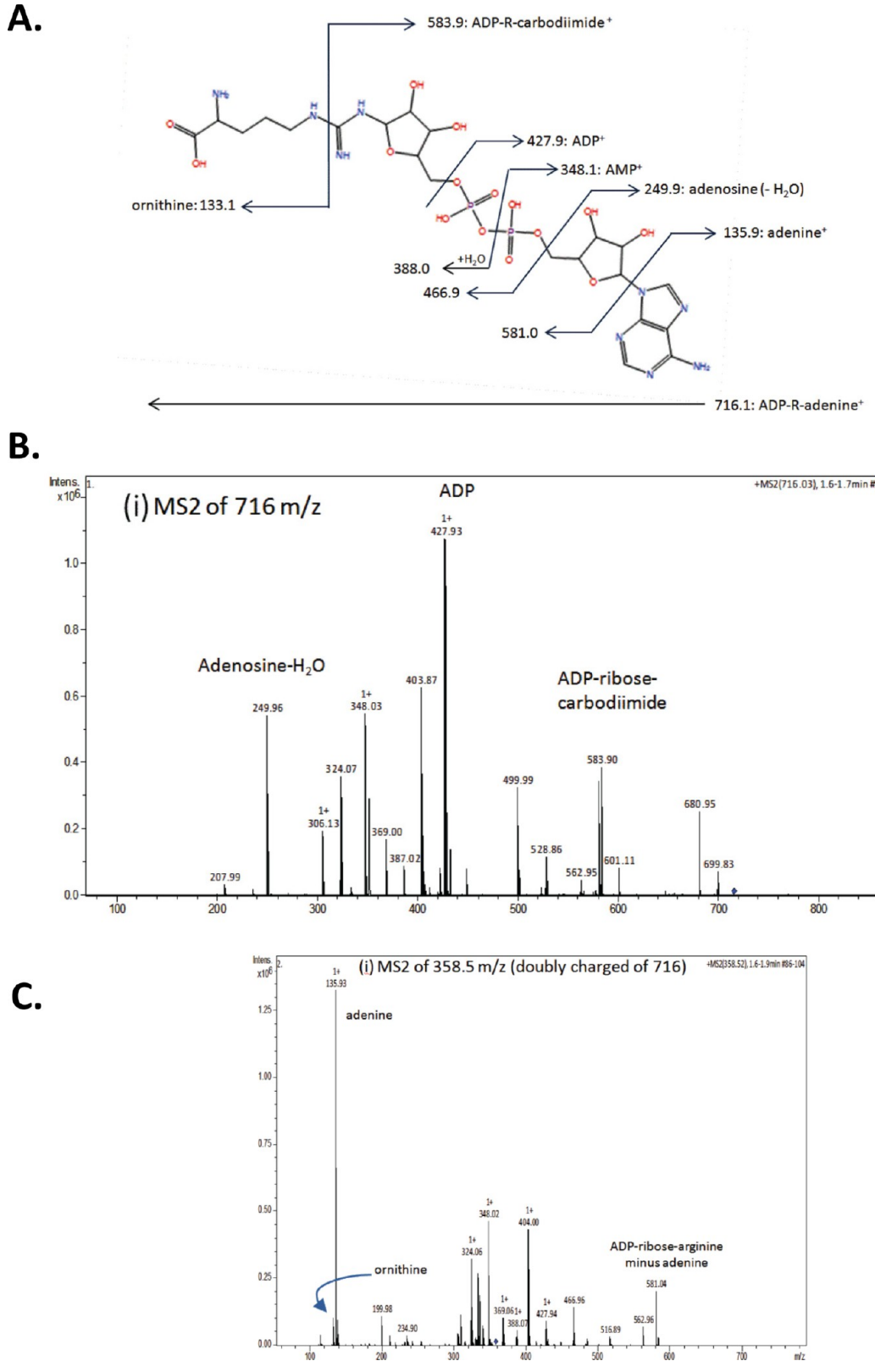

Figure 5. Mass spectrometry of the reaction products of Vis with L-arginine and NAD^+. (A) Product ion spectra of ADP-ribosyl-arginine in positive ion mode with product ion assignments. (B) Product ion spectra (singly charged, positive mode) after liquid chromatographic separation of the reaction products from the reaction of Vis with L-arginine and NAD^+. The entire spectrum is shown followed by expansion of the region corresponding to the ADP-ribose-carbodiimide species. (C) Product spectra (doubly charged, positive mode) after liquid chromatographic separation of the Vis reaction products. The entire spectrum is shown followed by expansion in the region corresponding to adenine and ornithine.

by Trp^{120}, Leu^{232}, and several water molecules, whereas the A-ribose is mostly stabilized by water molecules.

Vis NAD^+ Affinity. The Vis protein has five Trp residues (Trp^{44}, Trp^{51}, Trp^{88}, Trp^{120}, and Trp^{243}) in the full length

DOI: 10.1021/acs.biochem.5b00921
Biochemistry 2015, 54, 5920−5936

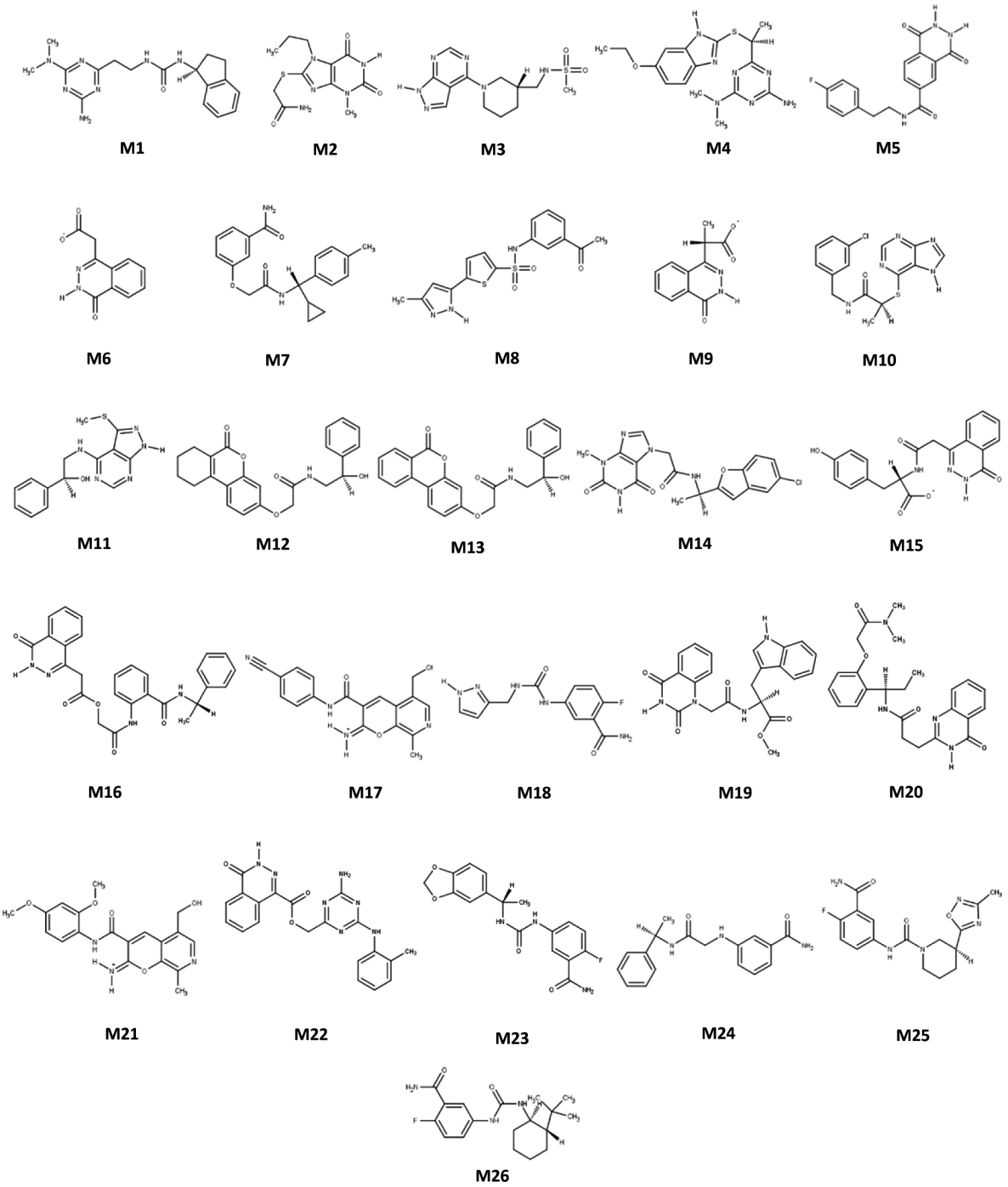

Figure 6. M-Series inhibitors tested against Vis ADP-ribosyltransferase activity. The top-scoring compounds derived from a virtual screen against iota toxin in complex with NADH (PDB entry 1GIQ) (designated the M-series) were chosen for experimental testing as inhibitors against Vis ADP-ribosyltransferase activity: M1, 1-{2-[4-amino-6-(dimethylamino)-1,3,5-triazin-2-yl]ethyl}-3-[(1*S*)-2,3-dihydro-1*H*-inden-1-yl]urea; M2, 2-[(3-methyl-2,6-dioxo-7-propyl-2,3,6,7-tetrahydro-1*H*-purin-8-yl)sulfanyl]acetamide; M3, *N*-{[(3*R*)-1-(1*H*-pyrazolo[3,4-*d*]pyrimidin-4-yl)piperidin-3-yl]-methyl}methanesulfonamide; M4, 6-{(1*S*)-1-[(6-ethoxy-1*H*-1,3-benzodiazol-2-yl)sulfanyl]ethyl}-N2,N2-dimethyl-1,3,5-triazine-2,4-diamine; M5, *N*-[2-(4-fluorophenyl)ethyl]-1,4-dioxo-1,2,3,4-tetrahydrophthalazine-6-carboxamide; M6, 2-(4-oxo-3,4-dihydrophthalazin-1-yl)acetate; M7, 3-({[(*S*)-cyclopropyl(4-methylphenyl)methyl]carbamoyl}methoxy)benzamide; M8, *N*-(3-acetylphenyl)-5-(3-methyl-1*H*-pyrazol-5-yl)thiophene-2-sulfonamide; M9, (2*S*)-2-(4-oxo-3,4-dihydrophthalazin-1-yl)propanoate; M10, (2*S*)-*N*-[(3-chlorophenyl)methyl]-2-(7*H*-purin-6-ylsulfanyl)propanamide; M11, (1*S*)-2-{[3-(methylsulfanyl)-1*H*-pyrazolo[3,4-*d*]pyrimidin-4-yl]amino}-1-phenylethan-1-ol; M12, *N*-[(2*R*)-2-hydroxy-2-phenylethyl]-2-[(6-oxo-6*H*,7*H*,8*H*,9*H*,10*H*-cyclohexa[*c*]chromen-3-yl)oxy]acetamide; M13, *N*-[(2*R*)-2-hydroxy-2-phenylethyl]-2-[(6-oxo-6*H*-benzo[*c*]chromen-3-yl)-oxy]acetamide; M14, *N*-[(1*R*)-1-(5-chloro-1-benzofuran-2-yl)ethyl]-2-(3-methyl-2,6-dioxo-2,3,6,7-tetrahydro-1*H*-purin-7-yl)acetamide; M15, (2*S*)-3-(4-hydroxyphenyl)-2-[2-(4-oxo-3,4-dihydrophthalazin-1-yl)acetamido]propanoate; M16, [(2-{[(1*S*)-1-phenylethyl]carbamoyl}phenyl)-carbamoyl]methyl 2-(4-oxo-3,4-dihydrophthalazin-1-yl)acetate; M17, 3-[(4-cyanophenyl)carbamoyl]-5-(hydroxymethyl)-8-methyl-2*H*-pyrano[2,3-*c*]pyridin-2-iminium; M18, 2-fluoro-5-{[(1*H*-pyrazol-3-ylmethyl)carbamoyl]amino}benzamide; M19, methyl-(2*S*)-2-[2-(2,4-dioxo-1,2,3,4-tetrahydroquinazolin-1-yl)acetamido]-3-(1*H*-indol-3-yl)propanoate; M20, *N*-[(1*R*)-1-{2- [(dimethylcarbamoyl)methoxy]phenyl}propyl]-3-(4-oxo-3,4-dihydroquinazolin-2-yl)propanamide; M21, 3-[(2,4-dimethoxyphenyl)carbamoyl]-5-(hydroxymethyl)-8-methyl-2*H*-pyrano[2,3-*c*]pyridin-2-iminium;

DOI: 10.1021/acs.biochem.5b00921
Biochemistry 2015, 54, 5920−5936

Figure 6. continued

M22, {4-amino-6-[(2-methylphenyl)amino]-1,3,5-triazin-2-yl}methyl 4-oxo-3,4-dihydrophthalazine-1-carboxylate; M23, 5-({[(1*S*)-1-(2*H*-1,3-benzodioxol-5-yl)ethyl]carbamoyl}amino)-2-fluorobenzamide; M24, 3-[({[(1*R*)-1-phenylethyl]carbamoyl}methyl)amino]benzamide; M25, (3*S*)-*N*-(3-carbamoyl-4-fluorophenyl)-3-(3-methyl-1,2,4-oxadiazol-5-yl)piperidine-1-carboxam; M26, 5-({[(1*R*,2*S*)-2-*tert*-butylcyclohexyl]carbamoyl}-amino)-2-fluorobenzamide.

Table 3. Comparison of K_d, IC_{50}, K_i, and Solubility Parameter Values for Inhibitors of *V. splendidus* Vis Toxin[a]

compd	K_d (μM)	K_i (μM)	IC_{50} (μM)	pIC_{50}[b]
M2	51 ± 12	25 ± 2	61 ± 5	4.2
M3	35 ± 7	90 ± 4	221 ± 10	3.7
M4	nd[c]	44 ± 6	108 ± 15	4.0
M6	nd[c]	74 ± 19	181 ± 47	3.7
M9	nd[c]	75 ± 11	184 ± 27	3.7
M10	7 ± 2	232 ± 51	568 ± 125	3.2
M15	162 ± 16	119 ± 27	292 ± 66	3.5
M18	4 ± 2	134 ± 20	328 ± 49	3.5
M19	35 ± 7	61 ± 10	150 ± 25	3.8
M24	0.2 ± 0.05	354 ± 91	867 ± 223	3.1
M25	0.7 ± 0.2	629 ± 154	1541 ± 377	2.8

[a]The binding affinity of inhibitors for WT $ExoA_c$ (K_d), the inhibition constant (K_i), and IC_{50} were calculated as described in Experimental Procedures. [b]The pIC_{50} values were calculated from the IC_{50} values as follows: $pIC_{50} = -\log IC_{50}$. The higher the pIC_{50} value, the smaller dose that is required for 50% inhibition of Vis toxin activity. [c]Not determined.

structure, but Trp^{243} was absent in the recombinant protein used in this study because of a C-terminal truncation (Pro^{20}–Ala^{240}), leaving only four potential Trp emitters. However, Trp^{44} and Trp^{51} are found in a highly solvent-exposed location within Vis, and hence, both are likely quenched through contact with solvent water molecules. This leaves only Trp^{88} and Trp^{120} as candidates for the observed Vis Trp fluorescence emission, which is quenched by 43% at saturating NAD^+ concentrations. Monitoring the WT Vis Trp fluorescence emission by titration with NAD^+ resulted in a binding isotherm described by a single K_d of 95 ± 7 μM (Figure 3D and Table 2), which is consistent with the known NAD^+ affinity for other mART toxins.[9,39,40] The NAD^+ binding ability for the Vis E189A/E191A double variant was also tested, resulting in an affinity similar to that of the WT toxin (Figure 3E). The Vis-NAD^+ structure (Figure 4A) shows that Trp^{120} is adjacent to the adenine-ribose of the NAD^+ (~7 Å between the indole-adenine centroids). The direct influence of NAD^+ on the electronic environment of Trp^{120} may be deduced from the significant electrostatic interaction energy, in addition to two H-bonds with its side chain (Figure 4A), strongly suggesting that Trp^{120} is the major (but not exclusive) reporter of the NAD^+ binding.

Vis GH Activity. The GH (NAD^+ase) activity in most mART enzymes is secondary and represents the transfer of ADP-ribose to water (OH^-) in the absence of a nucleophilic residue within a target protein.[21,41] Vis GH activity was characterized with a fluorescence-based assay developed in our laboratory using the fluorescent analogue εNAD^+ (Figure 4B).[42] Vis GH activity showed Michaelis–Menten behavior with a K_M of 276 ± 12 μM for εNAD^+ and a k_{cat} of (1.20 ± 0.03) × 10^{-3} min^{-1} (Table 2). These kinetic parameters for GH activity are similar to those reported for the C3 mART toxin subgroup.[43,44] The GH activity for the catalytic variant, E189A/E191A, was not detectable, even at a relatively high enzyme concentration (Figure 4B).

Vis ADP-Ribosylates Arginine-like Compounds. Arginine-specific mART toxins carry a characteristic catalytic signature that features the R-S···E-X-E motif that distinguishes these enzymes from structurally related enzymes that catalyze ADP ribosylation of other protein residues, guanine bases in DNA, or small molecule targets.[45] *In silico* analysis of Vis showed that it clearly falls within this subgroup of arginine-modifying enzymes (Figure 1A,B). To test this prediction, Vis was incubated with either L-arginine or agmatine; both have been previously used to characterize the mART activity of cholera[46] and pertussis toxins.[47] The mART activity of Vis in the presence of εNAD^+ and agmatine is shown in Figure 4C. Vis showed Michaelis–Menten behavior kinetics for the transfer of εADP-ribose to the synthetic substrate, agmatine, with a K_M of 272 ± 18 mM and a k_{cat} of 0.011 min^{-1}, which is ~10-fold higher than the GH activity of the toxin (Table 2). These results demonstrate that the ternary Vis-agmatine-εNAD^+ complex offers a "more favorable" conformation of the catalytic residues that accelerates the scission of the glycosidic bond in comparison to that of the binary Vis-εNAD^+ complex. However, the turnover number for Vis transferase activity against agmatine is considerably slower, for example, than that reported for C3larvin with the target rhoA protein (50-fold lower);[43] this observation is consistent with the slow binding step of agmatine to Vis (or to the Vis-εNAD^+ complex) as evidenced by the low enzyme efficiency (k_{cat}/K_M) for this synthetic substrate (Table 2). The mART activity for the catalytic variant, E189A/E191A, was not detectable, despite its ability to bind the NAD^+ substrate with an affinity similar to that of the WT toxin (Figure 3D,E).

Vis Transfers ADP-Ribose to the Guanidinium Group. To conclusively demonstrate that Vis transfers the ADPR moiety to the guanidinium side chain of L-arginine, NAD^+ and L-arginine were incubated with the enzyme at 25 °C overnight and the reaction products were separated by liquid chromatography (LC) followed by mass spectrometry in positive ion mode analysis (Figure 5). Unlabeled L-arginine showed the expected mass of 175 Da, whereas the ADP-ribosyl-arginine product arising from Vis enzymatic activity gave a mass of 716 Da. The spectrogram reported fragments compatible with a fragmentation pattern from the ADP-ribose moiety of the adduct ADP-ribosyl-arginine under the positive ion mode analysis (AMP^+, ADP^+, $adenine^+$, etc.). In addition to the presence of a fragment at m/z 133 representing ornithine, the complementary fragment at m/z 584 representing the ADP-ribose-carbodiimide indicates the covalent addition of ADP-ribose occurred at the guanidinium group of L-arginine,[48] and by extension for the agmatine substrate, as well. Notably, the amino group of L-arginine would be required to be deprotonated to act as a nucleophile. This provided strong evidence indicating that Vis does indeed recognize and label the arginine side chain as an R-S···E-X-E mART subgroup enzyme.

Inhibition of Vis Transferase Activity. Some compounds from an in-house library of 26 druglike molecules, designated as

DOI: 10.1021/acs.biochem.5b00921
Biochemistry 2015, 54, 5920–5936

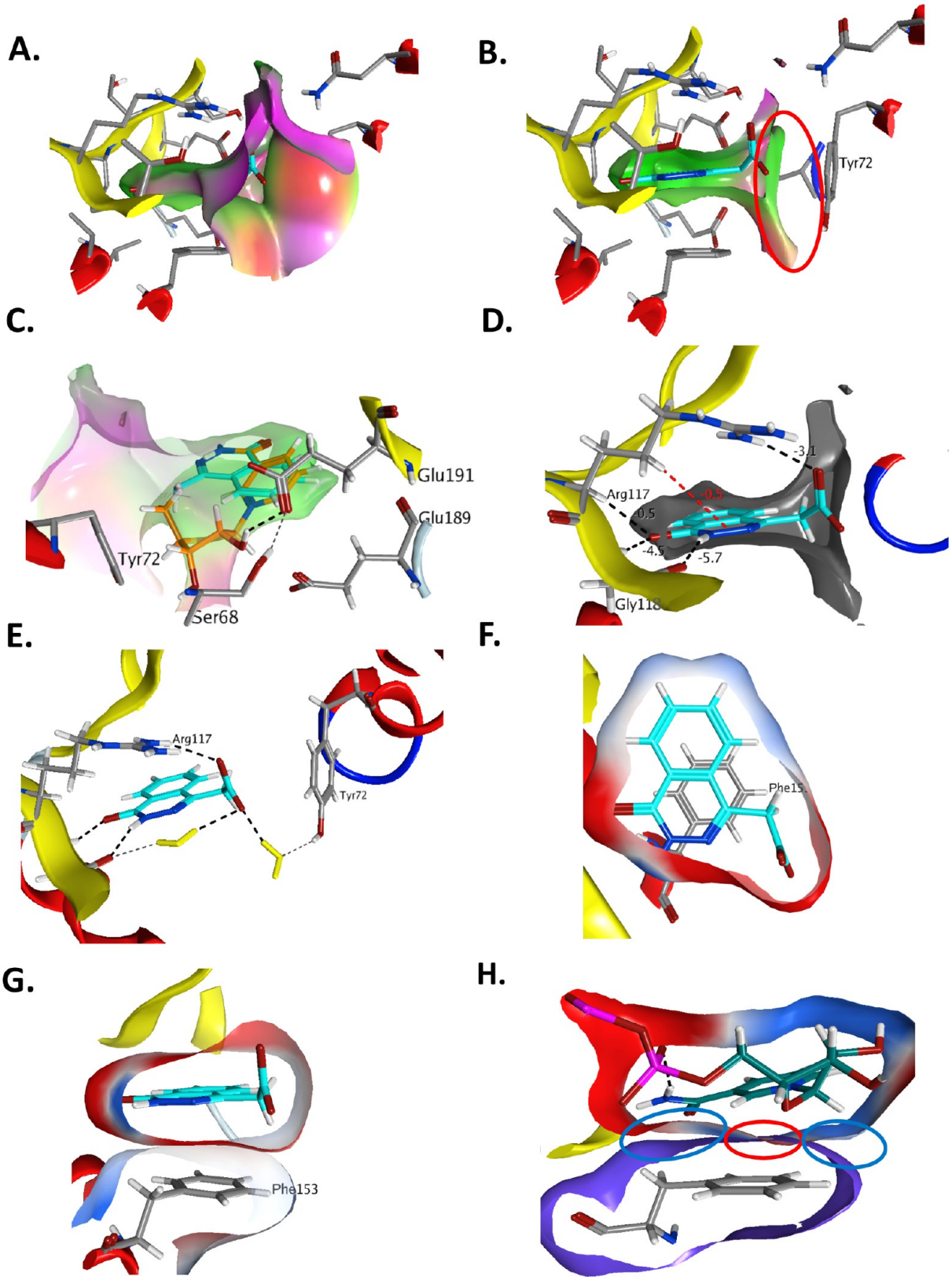

Figure 7. Interactions of Vis with M6 and NAD^+. Depiction of H-bonds and interacting surfaces between pocket Vis residues and M6 (in cyan C atoms, panels A–G) and NAD^+ (panel C and H). (A) Pocket residues defining the van der Waals surface around M6 in the Vis active site. (B) Slice of the surface in panel A, showing the flat volume at the N-subpocket that contains the ring system of M6, while the acetate carboxylate protrudes from the pocket. A marginal empty subcavity is observed in the proximity of Tyr^{172} (red oval). (C) Superposition of three main pharmacophore properties of the Vis receptor. Active pose of NAD^+ (C atoms colored orange) in the Vis-NAD^+ complex, overlaid onto the Vis-M6 pocket. (D) H-Bond network between M6 and Arg^{117} and Gly^{118} of Vis. Arg^{117} is an H-donor by three different H-bond types (including a H-Pi type, red dashed line), binding the ligand at three points. The numbers shown are the strengths of the H-bond interaction in kilocalories per mole. (E) Anchoring of

DOI: 10.1021/acs.biochem.5b00921
Biochemistry 2015, 54, 5920–5936

Figure 7. continued

the M6 tail by direct H-bonds with Arg^{117} and two water-mediated bridges with Gly^{118} (left) and Tyr^{72} (right). (F) Lateral view of Phe^{153} and M6 with their molecular surfaces colored by electrostatic potential (blue positive, red negative). (G) Upper view of Phe^{153} and M6 by 90° rotation of the perspective in panel F. (H) Lateral view of Phe^{153} and NAD^+ in the Vis-NAD^+ complex. The substrate and side chain moieties do not make good van der Waals contacts because their molecular surfaces either clash (red oval) or are not in contact (blue ovals). The figures were prepared using MOE (Molecular Operative Environment release 2014.08, Computational Chemistry Group, 2014).

the M-series and obtained from a previous virtual screening against iota toxin (PDB entry 1GIQ),[33] scored well in docking against the Vis structure from the Vis-NAD^+ complex (Figure 6). In effect, experimental testing of the M-series on Vis toxin revealed 11 compounds with appreciable activities (IC_{50} < 1 mM), including six compounds (M2−M4, M6, M9, and M19) with calculated K_i values of <100 μM, two compounds (M15 and M18) with K_i values of <150 μM, and the last three (M10, M24, and M25) with K_i values between 200 and 650 μM (Table 3). Compound M3 was previously shown to inhibit *Paenibacillus larvae* C3larvin toxin at a similar dosage.[43] Furthermore, 8 of 11 compounds induced quenching of the Vis Trp fluorescence upon binding, with estimated affinity on the same order of magnitude as the calculated K_i (i.e., 0.2 < K_d/K_i < 5). Four clear outliers correspond to compounds M10, M18, M24, and M25 (K_d/K_i < 0.05), where the weaker amplitude of the fluorescence quenching might have biased the fitting of the binding curve.

Interactions of Vis with M6 and NAD^+. M6 was the only M-series compound soaked into the Vis crystals that resulted in a high-resolution structure (Figures 6 and 7A−H). M6 is a two-ring, heterocyclic compound featuring a benzene ring fused to dihydropyridazinone from which protrudes an acetate substituent (Figure 6). Fifteen residues from the Vis protein form the van der Waals surface around the M6 ligand, and the occupied volume is essentially a flat pocket that is nearly closed and mostly inaccessible to the solvent (Figure 7A). The acetate substituent is in the vicinity of Tyr^{72}, but a void in the van der Waals contact can be seen (Figure 7B, red oval) that is normally occupied by the N-ribose of the NAD^+ substrate. The M6 benzene ring (Figure 7C, cyan atoms) overlaps with the nicotinamide ring of NAD^+ (orange atoms), although the latter adopts a tilted orientation within the nicotinamide pocket of the enzyme. The van der Waals surface of the methylene group of the Glu^{189} and Glu^{191} side chains [part of the E-X-E motif (Figure 1A)] contacts the hydrogens of the M6 benzene ring, while Tyr^{72} and Ser^{68} form the cavity to accommodate the N-ribose of the NAD^+ substrate (Figure 7C). Gly^{118} and Arg^{177} are key residues in the coordination of the M6 inhibitor (Figure 7D). The carbonyl and secondary amine of the dihydropyridazinone ring of M6 superposes almost perfectly with the nicotinamide amide of NAD^+ upon comparison of the Vis-NAD^+ and Vis-M6 structures. However, the backbone of Gly^{118} has a more favorable geometry with M6 than with NAD^+, making strong backbone H-bonds with the former (Gly^{118} carbonyl H-bond; $E_{H\text{-}bond}$ = −5.7 kcal/mol). Also, Arg^{177} plays an important role in stabilizing the acetate substituent of M6 through electrostatic and H-bond interactions with the terminal carboxylate, mimicking the interaction with the NAD^+ substrate. Furthermore, the M6 acetate carboxylate is bridged by two conserved water molecules with Gly^{118} and Tyr^{72} (Figure 7E). Moreover, the Phe^{153} side chain is parallel to the M6 ring system and makes favorable van der Waals contact mainly with the dihydropyridazinone ring (Figure 7F,G), an interaction that is not present in the Vis-NAD^+ complex (Figure 7G). On the contrary, in the Vis-NAD^+ structure, Phe^{153} shows some steric clashes in a part of the van der Waals surface (Figure 7H, red oval), with little or no contact in other parts (Figure 7H, blue ovals), which implies that the twisted N-ribose of NAD^+ poses a suboptimal geometry with Phe^{153}. In summary, the M6 ligand in Vis shows 15 heavy atoms that interact with 16 residues with an overall stabilization energy of −39.2 kcal/mol. In contrast, the N-moiety of NAD^+ (nicotinamide-ribose-phosphate) has 22 heavy atoms interacting with 16 Vis residues with −73 kcal/mol of stabilization energy. However, the interaction efficiency is only 30% higher for NAD^+ [−2.45 kcal mol^{-1} (heavy atom)$^{-1}$] than for M6 [−3.35 kcal mol^{-1} (heavy atom)$^{-1}$]. Importantly, the M6 ligand has only two rotatable bonds by which the entropic penalty due to binding within the Vis active site is negligible in relation to the NAD^+ N-moiety.

Structural Comparison of Vis and Iota Toxins. The optimal superposition of Vis and iota I_a toxins, the former in complex with NAD^+ and the latter with NAD^+ and actin,[49] allows a detailed comparison (Figure 8A). Although the same protein fold and scaffold structure exists for both toxins, the loop regions that are important for conferring regulation and/or substrate specificity are not well conserved in sequence or trajectory. In this sense, Iota I_a mediates recognition of actin through five loops within the enzyme: loop I (Tyr^{60}−Tyr^{62}), loop II ($\alpha2$−$\alpha3$ loop, Arg^{248}−Tyr^{251}), loop III ($\beta1$−$\beta2$ loop, Ser^{297}−Tyr^{311}), loop IV (PN loop, Met^{346}−Lys^{353}), and loop V (ARTT loop, Gly^{374}−Gly^{377}).[49] The N-terminal loop I, shown to be important for interaction with actin, does not exist within the Vis structure. The active-site loop between helices $\alpha2$ and $\alpha3$ (loop II) does superpose with the corresponding loop in Vis, but it does not share any common residues, although there is considerable conservation between the two toxins at helices $\alpha2$ and $\alpha3$, especially in the regions flanking the loop. Loop III in iota I_a toxin, located between $\beta1$ and $\beta2$, diverges in sequence, structure, and trajectory from the corresponding strands in Vis (Figure 8B). Loop IV (PN loop), found between $\beta3$ and $\beta4$, is considerably larger in Vis than in iota I_a (Figure 8C) and houses a short helix in Vis with the sequence E-V-A that resembles cholix toxin.[35] The second helix within the PN loop in Vis aligns in both toxins and contains the conserved Phe residue known to contact the nicotinamide moiety of NAD^+ (Figure 8C). Arg^{352} in the PN loop of iota is conserved among the actin-targeting toxins[49] but is replaced with a His residue in Vis toxin. Loop V (ARTT loop), situated between $\beta4$ and $\beta5$, is similar in length and follows the same trajectory for the two toxins. The long $\beta6$ and $\beta7$ strands in Vis overlap at the proximal end with iota I_a while diverging at the tip. Unique to Vis toxin is an additional long C-terminus with a β−loop−β motif with Tyr^{230} in the proximity of the adenine ring of NAD^+ (Figure 8D), although its role is currently unknown. In summary, even though the substrate specificity among actin-specific mARTs has not been clearly reconciled to date, it is clear that Vis is not a member of the actin-targeting mART toxins based upon the comparison with iota I_a toxin.

DOI: 10.1021/acs.biochem.5b00921
Biochemistry 2015, 54, 5920−5936

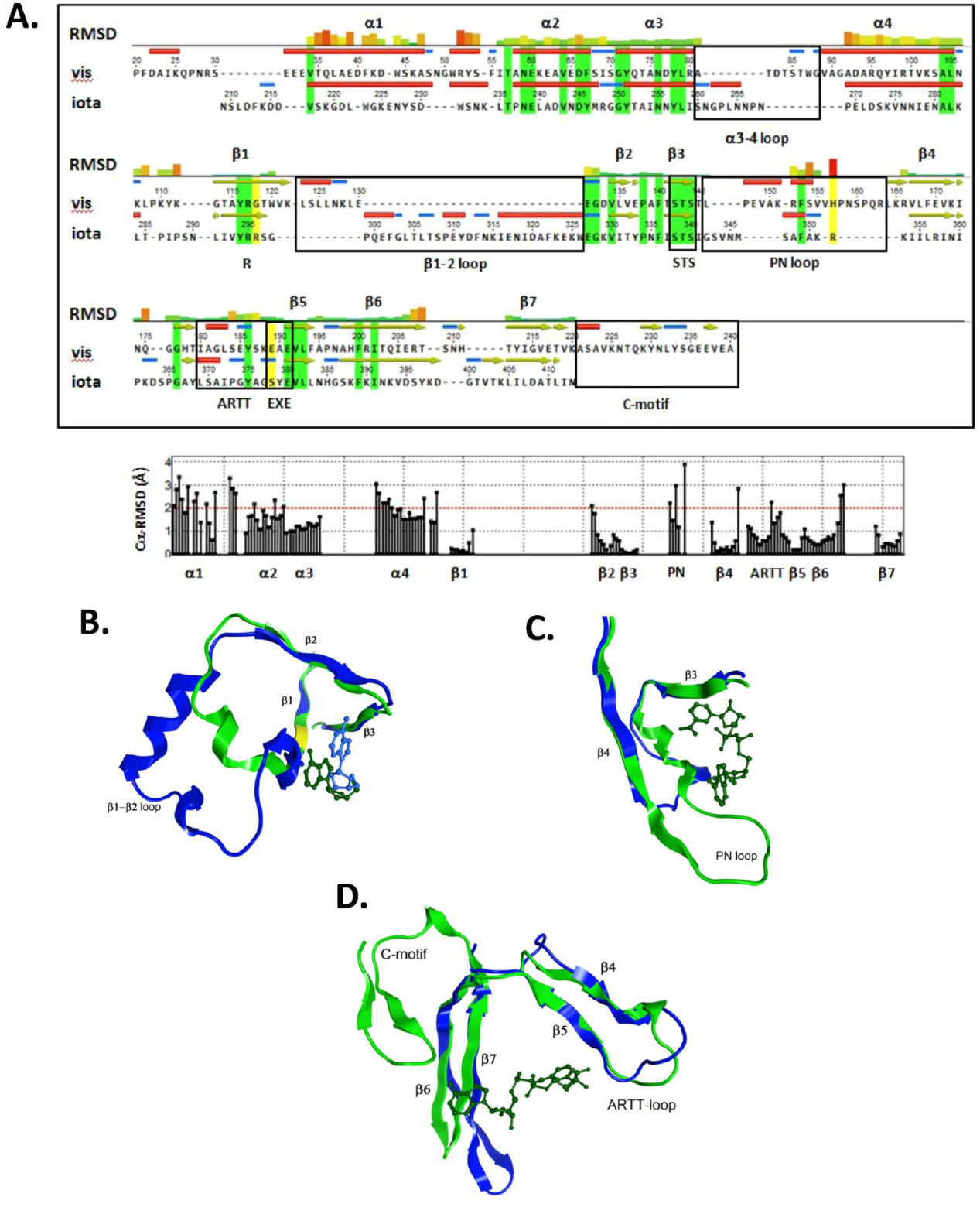

Figure 8. Sequence alignment of Vis and iota toxins complexed with NAD^+ based on structural superposition. (A) Alignment of Vis (PDB entry 4XZJ) and iota toxins (PDB entry 4HOV) based on the optimal superposition of the C_α atoms of 12 residues belonging to $\beta1-\beta3$ in Vis. In all panels, Vis-NAD^+ is colored green and iota-NAD^+ blue. (B) Core $\beta1-\beta3$. (C) PN loop. The PN loop is significantly longer in Vis than in iota, with a short α-helix with the sequence E-V-A at the N-terminus that resembles the same motif in cholix toxin. (D) ARTT loop and C-terminus. The short $\beta4$ and conserved $\beta5$ strands overlap well in both toxins. The ARTT loop has a similar length and follows the same trajectory for both Vis and iota I_a toxins.

Search for Vis Target(s). Recombinant Vis was first tested against known mART substrates such as actin (α, β, and γ), Rho GTPases (RhoA, RhoB, and RhoC), hRAS, proteins possessing the RNA recognition motif, etc. None of these proteins served as ADP-ribose acceptor proteins for the transferase activity of Vis (results not shown). A more extensive

DOI: 10.1021/acs.biochem.5b00921
Biochemistry 2015, 54, 5920−5936

substrate search was conducted using FLAG-tagged Vis against oyster lysate (*C. gigas*) in pull-down studies. The eluted samples were analyzed by ESI mass spectrometry. The top hits from the pull-down experiments included oyster actin (actin 2), retinol dehydrogenase, and various other proteins. These proteins were tested as potential substrates but yielded negative results as acceptors of ADP-ribose from Vis activity (results not shown). Thus, the E-X-E motif of Vis and the ability to modify the model substrate (arginine and agmatine) strongly indicate that it targets an Arg residue in its target protein;[45] however, currently, the identity of the natural target is not known.

DISCUSSION

In this study, Vis was identified as a novel mART toxin from *V. splendidus*, a well-known oyster pathogen[50] and a pathogen participating in gastroenteritis in humans.[51] The Vis enzyme is a hybrid among the VopT, C3, and C2 subgroups based on bioinformatics analysis (Figure 1A,B). A bioinformatics method[6,22] was used to discover Vis within the sequenced genome of *V. splendidus*, strain 12B01, a problematic oyster pathogen.[1,2,50] The Vis gene encodes a signal peptide (residues 1−19), indicating that it is a factor secreted by *V. splendidus* and a putative virulence factor. Vis was tested in a yeast assay and was shown to be toxic to the model eukaryotic organism when expressed in the cytoplasm under control of the weak CUP1 promoter (Figure 2A). Importantly, Vis catalytic variants (E189A, E191A, and E189A/E191A), designed to reduce or eliminate mART activity, showed reduced toxicity to the fungal host, indicating that Vis is indeed a mART toxin with enzymatically driven cytotoxicity in a eukaryotic cell host.

Several variants of Vis were expressed and purified in *E. coli* to find a stable and active protein until Pro^{20}−Ala^{240} was studied, which had its N-terminal signal sequence (residues 1−19) removed and nine residues from the C-terminus. Vis was shown to possess both GH (OH^- from water as the nucleophile) and transferase activities (Arg residue in a poly-Arg peptide, arginine, and agmatine; the latter is a known Arg-like substrate for mART toxins, as a nucleophile).[45] Vis showed weak GH activity, which was also observed for two other mART toxins grouped together with Vis (A. R. Merrill, unpublished observations).

Vis was shown to react with and label L-arginine and agmatine (an arginine analogue) with ADP-ribose (Figures 4C and 5), confirming the E-X-E motif is specific for arginine residues.[45] Unfortunately, we were unable to identify the target protein from oyster cell and mammalian cell lysates despite many trials involving affinity columns and pull-down assays. It seems that the target protein must exist at low abundance in the host cells but that it may be highly conserved because Vis was toxic to fungus (yeast) cells (Figure 2A). New strategies involving target enrichment in cell lysates combined with affinity methods, genetic knockout libraries, or SILAC experiments in yeast are required to determine the physiological target of Vis.

The crystal structure of Vis was determined in the absence of substrate or ligand (Vis-apo, 1.4 Å) and complexed with the NAD^+ substrate and M6 inhibitor (1.8 and 1.5 Å, respectively). The structures reveal that Vis is a single-domain mART toxin that folds into a mixed α/β structure with a classic mART fold that is C2/C3-like, but it also shows some resemblance to the ExoS subgroup. Vis has an unusual mART fold, as observed from the rmsd values in key regions of the catalytic domains of iota (2.80 Å, PDB entry 1GIQ), VahC (3.07 Å, PDB entry 4FML), and C3Bot1 (3.81 Å, PDB entry 2C89) toxins. The PN loop is longer and more extended in Vis than in other mART toxins such as those from the C2 and C3 subgroups, suggesting that Vis may recognize a unique target in host cells. This was supported by our target substrate experiments that showed that Vis does not react with conventional C2 and C3 protein substrates (actin, rho, etc.). Furthermore, Vis also has a shorter loop−helix region between its β1 and β2 strands that seems more like the VahC toxin from *Aeromonas hydrophila*.[9] A careful structural and sequence comparison of Vis with iota I_a and VahC toxins clearly showed that Vis is not a member of the actin-targeting mART toxin subgroup. In summary, our structural and biochemical data herein strongly suggest that Vis may indeed be a member of a new mART toxin subgroup, which we have termed Vis-like. Notably, our bioinformatics search strategy has already identified a second member of the Vis-like subgroup, which we are presently investigating.

Vis was tested against the top 26 hits from a library derived from a virtual screen against iota I_a toxin in complex with NAD^+ (Figure 6). Several of the compounds showed the ability to inhibit Vis mART activity against the agmatine substrate. These compounds are competitive inhibitors against the NAD^+ substrate and compete for the nicotinamide pocket within the enzyme (Table 3 and Figure 4D). These compounds share common features such as heterocyclic ring structures that can intercalate within the nicotinamide pocket and that also show good H-bonding capability with Vis active-site side chains (Figures 6 and 7). At present, we have only the cocrystal structure of Vis with M6, a lead inhibitor, which can be improved through rational drug design approaches.[52−54] Nevertheless, we are currently pursuing the crystal structures of several other M-series compounds with Vis.

Recently, our group has begun a serious pursuit to characterize the pharmacophore of the mART toxin active site using computational chemistry involving molecular dynamics simulations and energetic calculations.[55,56] The data from the study presented here will provide the basis for developing a specific pharmacophore structure tailored for the Vis-like mART toxin subgroup.

AUTHOR INFORMATION

Corresponding Author

*Department of Molecular and Cellular Biology, University of Guelph, Guelph, ON N1G 2W1, Canada. Telelphone: 519-824-4120, ext. 53806. Fax: 519-837-1802. E-mail: rmerrill@uoguelph.ca.

Funding

This work was supported by Canadian Institutes of Health Research Grant MOP-106661 (A.R.M.).

Notes

The authors declare no competing financial interest.

ACKNOWLEDGMENTS

We thank Dawn White and Tom Keeling for excellent technical assistance during the course of this study. We are grateful to Rob Gale and Ana Loncar for help in the initial stages of this research work. We are indebted to Drs. Wolfram Tempel and Hee-Won Park for assistance in collecting diffraction data from the in-house rotating anode facility at the Structural Genomics Consortium. Research in this paper was also performed using beamline 08ID-1 at the Canadian Light Source (Saskatoon, SK).

DOI: 10.1021/acs.biochem.5b00921
Biochemistry 2015, 54, 5920−5936

ABBREVIATIONS

εAMP, etheno-AMP; εNAD$^+$, etheno-NAD$^+$; GH, glycohydrolase; mART, mono-ADP-ribosyltransferase; rmsd, root-mean-square deviation; SD, standard deviation; WT, wild-type.

REFERENCES

(1) Gay, M., Berthe, F. C., and Le Roux, F. (2004) *Dis. Aquat. Org. 59*, 49−56.
(2) Le Roux, F., Zouine, M., Chakroun, N., Binesse, J., Saulnier, D., Bouchier, C., Zidane, N., Ma, L., Rusniok, C., Lajus, A., Buchrieser, C., Medigue, C., Polz, M. F., and Mazel, D. (2009) *Environ. Microbiol. 11*, 1959−1970.
(3) Fabioux, C., Pouvreau, S., Le Roux, F., and Huvet, A. (2004) *Biochem. Biophys. Res. Commun. 315*, 897−904.
(4) Deng, Q., and Barbieri, J. T. (2008) *Annu. Rev. Microbiol. 62*, 271−288.
(5) Holbourn, K. P., Shone, C. C., and Acharya, K. R. (2006) *FEBS J. 273*, 4579−4593.
(6) Fieldhouse, R. J., and Merrill, A. R. (2008) *Trends Biochem. Sci. 33*, 546−556.
(7) Aktories, K., Barmann, M., Ohishi, I., Tsuyama, S., Jakobs, K. H., and Habermann, E. (1986) *Nature 322*, 390−392.
(8) Vandekerckhove, J., Schering, B., Barmann, M., and Aktories, K. (1987) *FEBS Lett. 225*, 48−52.
(9) Shniffer, A., Visschedyk, D. D., Ravulapalli, R., Suarez, G., Turgeon, Z. J., Petrie, A. A., Chopra, A. K., and Merrill, A. R. (2012) *J. Biol. Chem. 287*, 37030−37041.
(10) Visschedyk, D. D., Perieteanu, A. A., Turgeon, Z. J., Fieldhouse, R. J., Dawson, J. F., and Merrill, A. R. (2010) *J. Biol. Chem. 285*, 13525−13534.
(11) Aktories, K., Rosener, S., Blaschke, U., and Chhatwal, G. S. (1988) *Eur. J. Biochem. 172*, 445−450.
(12) Nemoto, Y., Namba, T., Kozaki, S., and Narumiya, S. (1991) *J. Biol. Chem. 266*, 19312−19319.
(13) Just, I., Mohr, C., Schallehn, G., Menard, L., Didsbury, J. R., Vandekerckhove, J., van, D. J., and Aktories, K. (1992) *J. Biol. Chem. 267*, 10274−10280.
(14) Wilde, C., Just, I., and Aktories, K. (2002) *Biochemistry 41*, 1539−1544.
(15) Yamaguchi, T., Hayashi, T., Takami, H., Ohnishi, M., Murata, T., Nakayama, K., Asakawa, K., Ohara, M., Komatsuzawa, H., and Sugai, M. (2001) *Infect. Immun. 69*, 7760−7771.
(16) Yamaguchi, T., Nishifuji, K., Sasaki, M., Fudaba, Y., Aepfelbacher, M., Takata, T., Ohara, M., Komatsuzawa, H., Amagai, M., and Sugai, M. (2002) *Infect. Immun. 70*, 5835−5845.
(17) Barth, H., Preiss, J. C., Hofmann, F., and Aktories, K. (1998) *J. Biol. Chem. 273*, 29506−29511.
(18) Han, S., Craig, J. A., Putnam, C. D., Carozzi, N. B., and Tainer, J. A. (1999) *Nat. Struct. Biol. 6*, 932−936.
(19) Jørgensen, R., Wang, Y., Visschedyk, D., and Merrill, A. R. (2008) *EMBO Rep. 9*, 802−809.
(20) Sakurai, J., Nagahama, M., Hisatsune, J., Katunuma, N., and Tsuge, H. (2003) *Adv. Enzyme Regul. 43*, 361−377.
(21) Yates, S. P., Jørgensen, R., Andersen, G. R., and Merrill, A. R. (2006) *Trends Biochem. Sci. 31*, 123−133.
(22) Fieldhouse, R. J., Turgeon, Z., White, D., and Merrill, A. R. (2010) *PLoS Comput. Biol. 6*, e1001029.
(23) Adams, P. D., Grosse-Kunstleve, R. W., Hung, L. W., Ioerger, T. R., McCoy, A. J., Moriarty, N. W., Read, R. J., Sacchettini, J. C., Sauter, N. K., and Terwilliger, T. C. (2002) *Acta Crystallogr., Sect. D: Biol. Crystallogr. 58*, 1948−1954.
(24) Kabsch, W. (2010) *Acta Crystallogr., Sect. D: Biol. Crystallogr. 66*, 125−132.
(25) Jones, T. A., Zou, J. Y., Cowan, S. W., and Kjeldgaard, M. (1991) *Acta Crystallogr., Sect. A: Found. Crystallogr. 47*, 110−119.
(26) Emsley, P., and Cowtan, K. (2004) *Acta Crystallogr., Sect. D: Biol. Crystallogr. 60*, 2126−2132.
(27) Armstrong, S., and Merrill, A. R. (2001) *Anal. Biochem. 292*, 26−33.
(28) Turgeon, Z., White, D., Jørgensen, R., Visschedyk, D., Fieldhouse, R. J., Mangroo, D., and Merrill, A. R. (2009) *FEMS Microbiol. Lett. 300*, 97−106.
(29) Cheng, Y., and Prusoff, W. H. (1973) *Biochem. Pharmacol. 22*, 3099−3108.
(30) Armstrong, S., Li, J. H., Zhang, J., and Merrill, A. R. (2002) *J. Enzyme Inhib. Med. Chem. 17*, 235−246.
(31) Yates, S. P., Taylor, P. L., Jørgensen, R., Ferraris, D., Zhang, J., Andersen, G. R., and Merrill, A. R. (2005) *Biochem. J. 385*, 667−675.
(32) Barbieri, J. T., and Sun, J. (2005) *Rev. Physiol Biochem. Pharmacol. 152*, 79−92.
(33) Schleberger, C., Hochmann, H., Barth, H., Aktories, K., and Schulz, G. E. (2006) *J. Mol. Biol. 364*, 705−715.
(34) Jucovic, M., Walters, F. S., Warren, G. W., Palekar, N. V., and Chen, J. S. (2008) *Protein Eng., Des. Sel. 21*, 631−638.
(35) Fieldhouse, R. J., Jorgensen, R., Lugo, M. R., and Merrill, A. R. (2012) *J. Biol. Chem. 287*, 21176−21188.
(36) Bell, C. E., Yeates, T. O., and Eisenberg, D. (1997) *Protein Sci. 6*, 2084−2096.
(37) Jørgensen, R., Merrill, A. R., Yates, S. P., Marquez, V. E., Schwan, A. L., Boesen, T., and Andersen, G. R. (2005) *Nature 436*, 979−984.
(38) Menetrey, J., Flatau, G., Stura, E. A., Charbonnier, J. B., Gas, F., Teulon, J. M., Le Du, M. H., Boquet, P., and Menez, A. (2002) *J. Biol. Chem. 277*, 30950−30957.
(39) Visschedyk, D., Rochon, A., Tempel, W., Dimov, S., Park, H. W., and Merrill, A. R. (2012) *J. Biol. Chem. 287*, 41089−41102.
(40) Jorgensen, R., Purdy, A. E., Fieldhouse, R. J., Kimber, M. S., Bartlett, D. H., and Merrill, A. R. (2008) *J. Biol. Chem. 283*, 10671−10678.
(41) Yates, S. P., and Merrill, A. R. (2005) *Anal. Biochem. 340*, 41−51.
(42) Armstrong, S., and Merrill, A. R. (2001) *Anal. Biochem. 292*, 26−33.
(43) Krska, D., Ravulapalli, R., Fieldhouse, R. J., Lugo, M. R., and Merrill, A. R. (2015) *J. Biol. Chem. 290*, 1639−1653.
(44) Bohmer, J., Jung, M., Sehr, P., Fritz, G., Popoff, M., Just, I., and Aktories, K. (1996) *Biochemistry 35*, 282−289.
(45) Laing, S., Unger, M., Koch-Nolte, F., and Haag, F. (2011) *Amino Acids 41*, 257−269.
(46) Vichi, A., Moss, J., and Vaughan, M. (2005) *Methods Enzymol. 404*, 195−206.
(47) Gadkari, T. V., Cortes, N., Madrasi, K., Tsoukias, N. M., and Joshi, M. S. (2013) *Nitric Oxide 35*, 65−71.
(48) Osago, H., Yamada, K., Shibata, T., Yoshino, K., Hara, N., and Tsuchiya, M. (2009) *Anal. Biochem. 393*, 248−254.
(49) Tsuge, H., Nagahama, M., Oda, M., Iwamoto, S., Utsunomiya, H., Marquez, V. E., Katunuma, N., Nishizawa, M., and Sakurai, J. (2008) *Proc. Natl. Acad. Sci. U. S. A. 105*, 7399−7404.
(50) Rojas, R., Miranda, C. D., Opazo, R., and Romero, J. (2015) *J. Invertebr. Pathol. 124*, 61−69.
(51) Vezzulli, L., Pezzati, E., Stauder, M., Stagnaro, L., Venier, P., and Pruzzo, C. (2015) *Environ. Microbiol. 17*, 1065.
(52) Nepali, K., Sharma, S., Sharma, M., Bedi, P. M., and Dhar, K. L. (2014) *Eur. J. Med. Chem. 77*, 422−487.
(53) Keck, T. M., Burzynski, C., Shi, L., and Newman, A. H. (2014) *Adv. Pharmacol. 69*, 267−300.
(54) Nestorovich, E. M., and Bezrukov, S. M. (2014) *Expert Opin. Drug Discovery 9*, 299−318.
(55) Lugo, M. R., and Merrill, A. R. (2015) *J. Mol. Recognit. 28*, 539.
(56) Lugo, M. R., and Merrill, A. R. (2015) *J. Biomol. Struct. Dyn.*, 1−17.
(57) Gouet, P., Courcelle, E., Stuart, D. I., and Metoz, F. (1999) *Bioinformatics 15*, 305−308.
(58) Larkin, M. A., Blackshields, G., Brown, N. P., Chenna, R., McGettigan, P. A., McWilliam, H., Valentin, F., Wallace, I. M., Wilm,

DOI: 10.1021/acs.biochem.5b00921
Biochemistry 2015, 54, 5920−5936

A., Lopez, R., Thompson, J. D., Gibson, T. J., and Higgins, D. G. (2007) *Bioinformatics 23*, 2947−2948.

DOI: 10.1021/acs.biochem.5b00921
Biochemistry 2015, 54, 5920−5936